INVESTIGATING THE MECHANICAL PROPERTIES OF ALUMINUM AND EPOXY POLYMER USING MOLECULAR DYNAMICS SIMULATIONS

By © Douglas R. Pratt

A Thesis submitted to the

School of Graduate Studies in partial fulfillment of

the requirements for the degree of

Master of Engineering

Memorial University of Newfoundland

May 2020

St. John's Newfoundland

Abstract

Molecular Dynamics simulations were used to recreate mechanical testing procedures and to predict the mechanical properties of aluminum and epoxy polymers. In the first study, a procedure for performing nanoindentation on single crystal FCC aluminum was designed and used to test which available force field and parameter sets were best suited for accurately predicting the elastic modulus. The modulus was calculated from the generated force-displacement curve using Oliver & Pharr as well as Hertz indentation theory. The results were compared to literature data of single crystal aluminum and concluded the Embedded-Atom Method force field was the most accurate parameter model. The second study used Molecular Dynamics to simulate the curing of epoxy resins with a hardener to compare the effect of crosslinking reaction completion on the polymer's predicted mechanical properties obtained from a uniaxial tensile test. Results were compared to experimental results of the same epoxy polymer. The work concluded that the cure rate had a significant influence on the elastic modulus and density, while little effect on Poisson's ratio.

Acknowledgements

First and foremost, I would like to acknowledge my supervisor Dr. Sam Nakhla for his support and guidance through this program. He continuously challenged me to do more than I thought I could do over these two years and gave me the motivation I needed to complete the work presented in this thesis. I believe I am a much stronger engineer from being part of his team. Thank you for being an excellent supervisor. This program has been an invaluable experience for both my understanding of engineering and for the friendships I have made working in this group.

To my parents, I am grateful for their constant encouragement throughout my university career. They have instilled in me a strong drive for academics that has been the driving force for me to pursue my undergrad and graduate degrees. I am thankful for their unconditional support they have given me over these years.

To my coworkers, Liam, Stephen, Sabir and Ruby, I would like to thank them for the great friendships we have formed over these years and for their guidance throughout this program.

Finally, I would like to thank Bombardier for their financial contributions that allowed me to pursue this degree.

Contents

Table of Figures

List of Abbreviations and Symbols

MD – Molecular Dynamics

AFM – Atomic Force Microscopy

HCP – Hexagonally Close Packed

IR – Infrared

FCC – Face Centered Cubic

EAM – Embedded-atom Method

MEAM – Modified Embedded-atom Method

O&P – Oliver and Pharr

BCC – Body Centered Cubic

nN – nano Newton

Å – Angstrom

ps – picosecond

Al – Aluminum

DGEBA – Bisphenol A diglycidyl ether

DETDA – Diethyltoluenediamine

DETA – diethylene triamine (DETA),

TETA – triethylenetetramine

CVFF – Consistent Valence Force Field

fs – femtosecond

ns – nanosecond

mPs – millipascal-second

° – degree

GPa – Gigapascal

atm – atmosphere

DIC – digital image correlation

1. Chapter 1: Introduction

1.1 Background of Molecular Dynamics

In recent years, Molecular Dynamics (MD) simulations have been used to study and model the behaviour of metal and polymer systems at the atomistic length scale. Over the past decades the power of computational resources used for MD simulations has increased exponentially and has allowed for MD models to simulate systems with thousands of atoms. This allows for atomistic simulations to model the behaviour of microscale phenomena like dislocation behaviour and elastic/plastic deformation pathways [1]. This is particularly useful for modelling small materials or thin films, where traditional experimental testing cannot achieve the length scale required to describe the material behavior.

Molecular Dynamic simulations work by calculating the attractive and repulsive energies between neighboring atoms, which is then used to update each atom's position and velocity over successive time steps. The energy interactions are determined by a set of parameters called the force field. Force fields are created for the specific material, such as pure aluminum or epoxy polymer, and the parameters can be tuned based on empirical data or first-principle (ab-initio) calculations. Because of the inherent complexity of designing a parameter set that accurately predicts all natural phenomena a material can present, force fields will be designed to focus on a particular area, whether for certain mechanical properties, chemical pathways, or lattice arrangements. With a force field tuned for a certain material and its properties of interest, it is possible to use MD to recreate testing procedures to predict mechanical properties. Two areas where MD modelling would prove useful are the nanoindentation testing procedure and polymer modelling, which are discussed in the following two sections.

1.2 MD Simulations of Nanoindentation

Nanoindentation as a technique has been used for materials testing since the 1970s. As described by Lucca [2], nanoindentation is “based on the continuous recording of applied force and resulting depth of penetration of an indenter throughout the whole loading and unloading cycle.” It can also be performed as a displacement-controlled indentation, where the indenter speed is constant and the resulting force is recorded. As the name suggests it is used on extremely small length scales in the micro- and nanometer region making it useful for testing on thin films and small volume samples. Since then much work has gone into developing models and understanding of the nanoindentation contact mechanics. With the increasing sensitivity of atomic force microscopy (AFM) it is now possible to calculate forces and indentation depths on the scale of nanometers, allowing the use of incredibly small samples to determine mechanical properties [3]. The Oliver & Pharr [4] method uses the generated force-displacement curves to determine the elastic modulus and hardness from the material.

Since the nanoindentation occurs on such a small length scale, atomistic models become worth considering as Molecular Dynamics are performed at similar sizes. Atomistic modelling can be used to describe mechanical, chemical, dislocation and plastic deformation pathways that are not observable or describable from experimental results [3]. For instance, the work done by Fang and Wu [5] used MD to model the plastic deformation pathways and jump-contact behavior of aluminum-nickel multi-layered films. Their work showed how the atom-atom adhesion between the indenter and sample was a significant force governing the elastic behavior when the indenter is being detracted. This force is something that could not be resolved or studied from experimental behavior. In another work, Alhafez et al. [6] performed atomistic simulations to show how surface crystallography affected the dislocations formed during indentation. This study created a model to explain why the surface crystal orientation of hexagonal close packed (HCP) materials caused a significant effect on the resultant plastic zone during indentation, which cannot be observed through actual experimentation.

1.3 MD Simulations of Epoxy Polymers

Epoxy polymers and composites are used in a wide variety of materials and applications due to their excellent thermomechanical properties and low densities [7]. These polymers are commonly used in the aerospace industry as protective coatings and for corrosion resistance [7]. An epoxy polymer's material properties are of course directly related to the chemical structure of its resin and its curing agent, making the material a great candidate for molecular modelling using MD. Polymer design through experimental testing can be very expensive and time-consuming to research because of the time it takes for preparing, curing and testing different resins, curing agents and mixing ratios [8]. MD simulations offer the ability to examine different polymer structures using computation resources, which can result in faster, cheaper research with no chemical waste. The work by Fu et al. [9] used molecular dynamics to investigate the effect different anhydride curing agents had on mechanical properties which agreed well with experimental results. MD simulations also offer crosslinking structure information that can't be easily quantitated through experimental means. For example, the crosslink density, or the percent completion of the crosslinking reaction can only be qualitatively estimated through spectroscopic techniques like infrared (IR) [10]. Atomistic models however can produce an exact crosslink density and show the effect of cure rate directly on mechanical properties like modulus, density and Poisson's ratio.

1.4 Thesis Overview and Purpose

As evident from the previous discussions, molecular dynamics offers a wide range of ability to model a variety of different materials and simulate their behavior and mechanical properties during a virtual testing simulation. A quantified model for material testing would have key advantages over performing an actual experimental procedure. One such advantage is the cost savings associated to using a computer rather than paying the material and equipment costs associated to lab testing. Another is the full control of the material's environment, allowing the user to test a sample's mechanical properties in a setting that is difficult or costly to recreate in real life such as extreme temperatures and pressures. For these reasons, the author focused on using MD to design simulation procedures for common mechanical tests and compare the accuracy of their results to experimental data. This work investigates the performance of nanoindentation and tensile testing simulations.

The purpose of this thesis is to investigate the effectiveness of molecular dynamic simulations in predicting mechanical properties of aluminum and epoxy materials. In order to achieve this, first a Molecular Dynamics nanoindentation simulation procedure was designed and used to see which available force fields in the literature can most aptly predict the elastic modulus from the simulated indentation curves. The epoxy polymer models were also simulated using Molecular Dynamics. Epoxy resin and curing agent monomers were modelled and a crosslinking procedure was designed to create several epoxy samples at different degrees of cure. The predicted mechanical properties were compared to experimental data from a tensile test carried out using a load frame and high precision non-contacting strain measurement.

This thesis is written in manuscript format and contains four chapters. The first chapter is an overview of the background literature and purpose of this work. The second chapter is on simulating a nanoindentation procedure on an aluminum substrate and comparing the performance of several different aluminum force fields. The work also compares the accuracy of two different mathematical models for extracting modulus from nanoindentation curves. The third chapter discusses the design and procedure of modelling the crosslinking reaction of epoxy polymers and performing a tensile test to extract its mechanical properties. The model shows how Young's Modulus, Poisson's ratio and density as a function of degree of cure. These predicted values are compared to the experimental results of the same epoxy collected through a tension test by a load frame. Lastly, the fourth chapter is a summary of conclusions from the two works discussed in this thesis.

1.5 Co-authorship Statement

The following sections of this thesis were collaborative works. The purpose of this section is to highlight the contributions made by each co-author.

In the second chapter, the paper titled *Molecular Dynamics Simulations of Nanoindentation – The Importance of Force Field Choice on the Predicted Elastic Modulus of FCC Aluminum*, contributions were made by Liam Morrisey. The initial research literature review, simulation design, data analysis and manuscript preparation were done by the author of this thesis. Morrisey provided help in validating the results obtained from the simulation.

In the third chapter, the paper titled *Molecular Dynamics Study on the Mechanical Properties of the DGEBA/DETDA Polymer System*, contributions were made by Ahmed Youssri Elruby. The initial research literature review, simulation design, simulation data analysis and manuscript preparation were completed by the author of this thesis. Elruby was responsible for performing and analyzing the experimental results in which the molecular model was compared with.

References

[1] D. Farkas, "Atomistic simulations of metallic microstructures," *Current Opinion in Solid State and Materials Science,* vol. 17, *(6),* pp. 284-297, 2013.

[2] D. A. Lucca, K. Herrmann and M. J. Klopfstein, "Nanoindentation: Measuring methods and applications," *CIRP Ann. Manuf. Technol.,* vol. 59, *(2),* pp. 803-819, 2010. . DOI: 10.1016/j.cirp.2010.05.009.

[3] R. F. Gibson, "A Review of Recent Research on Nanoindentation of Polymer Composites and their Constituents," *Composites Sci. Technol.,* vol. 105, pp. 51-65, 2014.

[4] W. C. Oliver, "An Improved Technique for Determining Hardness and Elastic Modulus using Load and Displacement Sensing Indentation Experiments," *J. Mater. Res.,* vol. 7, *(6),* 1992.

[5] T. Fang and J. Wu, "Molecular Dynamics Simulations on Nanoindentation Mechanisms of Multilayered Films," *Computational Materials Science,* vol. 43, *(4),* pp. 785-790, 2008.

[6] I. A. Alhafez *et al*, "Nanoindentation of HCP Metals: A Comparative Simulation Study of the Evolution of Dislocation Networks," *Nanotechnology,* vol. 27, *(4),* pp. 045706, 2015.

[7] J. L. Massingill and R. S. Bauer, "Epoxy Resins," in Craver C.D.; Carraher Jr. C.E., Eds, Applied Polymer Science 21st Century, Elsevier, Amsterdam, pp. 393-424, 2000. . DOI: https://doi.org/10.1016/B978-008043417-9/50023-4.

[8] F. Jeyranpour, G. Alahyarizadeh and B. Arab, "Comparative Investigation of Thermal and Mechanical Properties of Cross-Linked Epoxy polymers with Different Curing Agents by Molecular Dynamics Simulation," *J. Mol. Graph. Model.,* vol. 62, pp. 157-164, 2015.

[9] K. Fu *et al*, "Molecular Dynamics Simulation and Experimental Studies on the Thermomechanical Properties of Epoxy Resin with Different Anhydride Curing Agents," *Polymers,* vol. 11, pp. 975, 2019. . DOI: 10.3390/polym11060975.

[10] I. Yarovsky and E. Evans, "Computer Simulation of Structure and Properties of Crosslinked Polymers: Application to Epoxy Resins" *Polymer,* vol. 43, *(3),* pp. 963-969, 2002.

2. Chapter 2: Molecular Dynamic Simulations of Nanoindentation –The Importance of Force Field Choice on the Predicted Elastic Modulus of FCC Aluminum

Abstract: Molecular Dynamics (MD) simulations are performed to simulate nanoindentation tests in order to calculate macroscale properties on the atomistic scale. Care must be taken that the force field potential used in MD simulations is appropriate for the application. In this work, nanoindentation was simulated using three different types of force fields to test their accuracy in predicting elastic modulus of aluminum. The force fields chosen were the Embedded-atom method (EAM), the modified Embedded-atom method (MEAM) and the ReaxFF potential. The results showed that EAM type force fields are in reasonable agreement with experimental nanoindentation results, while the MEAM and ReaxFF potentials had significant error. The importance of choosing a potential based on its type and the application of its parameter set is discussed. Two different methods for calculating modulus from indentation curves were compared: The Hertz approximation and the Oliver and Pharr (O&P) method. For EAM and MEAM force fields, the Hertz method significantly under predicted modulus while the O&P method tended to over predict. For ReaxFF the two methods were in good agreement with each other.

Note: This paper is currently in submission. Ref: Pratt, D.R., Morrissey, L.S. and Nakhla, S., “Molecular Dyamic Simulations of Nanoindentation – The importance of Force Field

Choice on the Predicted Elastic Modulus of FCC Aluminum”, Journal of Molecular Simulations, (Submitted).

2.1 Introduction

The field of Molecular Dynamics (MD) has been gaining considerable interest in the areas of material science and engineering. Once limited to chemical applications, advances in computational resources have allowed typical material property tests to be recreated at the atomistic level [1]. Now, this method is able to predict macroscale properties of metals and thin layer systems, providing models for dislocation and chemical pathways on the atomic scale [2]. MD simulations are particularly useful for nanoindentation testing where their length-scales are similar, allowing for MD to model defect formation that is otherwise difficult by more traditional methods [3]. For instance, Lilleoden et al. used nanoindentation MD simulations to compare dislocations in single crystal gold as a function of the indenter's position relative to grain boundaries which could not be simply measured in an actual nanoindentation test [4]. This in turn allowed insight into how the sample forms dislocations and deforms on the atomistic level throughout the loading procedure. Christopher and Richter used MD to show the piling-up and sinking-in effects during nanoindentation. Their work compared simulations to experimental data of iron and silver to provide models for piling-up during the indentation process. Their simulation results not only had good agreement with the piling-up observed from their indentation of iron and silver, but also provided a sub-surface model of dislocations pathways in BCC and FCC structures [5]. Finally, MD simulations can also allow tracking of chemical reactions that can occur during testing. Stewart and Spearot were able to use computational models to show the changes in chemical structure and phase on films of molybdenum sulfide lubricants as the indenter lowered [6].

Due to the atomistic mechanisms of dislocations and yield involved during nanoindentation being only observable through the simulations, it is crucial to ensure the material's behavior is being properly simulated. As a consequence, much of the literature on nanoindentation focuses on the effects of different simulation design parameters then optimizing them for the prediction of mechanical properties. For instance, Nair et al. performed studies on the effect of the indenter's velocity, shape and radius on the estimated hardness and modulus of nickel thin films [7]. In another work, Goel et al. showed the effect of different indenter models on the measured hardness of tungsten [8]. Moreover, beyond these test variables there are other MD specific variables that must also be considered. For example, Yaghoobi and Voyiadjis simulated the effects of different boundary conditions used in nanoindentation simulations, such as periodic, non-periodic and configurations of frozen atoms [9]. Results showed that as the simulation's thickness becomes large compared to the radius of the indenter, the effect of the chosen boundary conditions on the predicted modulus becomes negligible.

However, one MD variable that is seldom discussed in the literature for nanoindentation simulations is the choice of force field to be used. The force field determines how the simulation calculates atom-atom interactions like attraction, repulsion and packing structure. Despite the variety of force field types available, there have only been limited studies that compare the performance of different potentials in predicting mechanical properties through nanoindentation simulations. The work by Nair et al. shows how significant the results can differ by changing the force field. They found that using two different force fields for nickel indentation caused their predicted modulus to change by

20%, meanwhile they did not make a conclusion as to which potential is more accurate [7]. A comparative study by Rassoulinejad-Mousavi et al. was performed to test the accuracy of elastic constants predicted by potentials for copper, nickel and aluminum through tensile tests [10]. Their work determined that while some force fields can accurately predict one or two elastic constants, no single potential was precise for all applications. This presents a need to test the available potentials in nanoindentation in order to determine their performance specifically for nanoindentation. Therefore, the goal of this research was to examine several potentials from three different force field types: Embedded-atom method (EAM), modified Embedded-atom method (MEAM) and ReaxFF and their prediction of the elastic modulus of aluminum in order to show which force field is the optimal choice for nanoindentation simulations.

2.2 MD Simulation Procedure

The MD simulations in this experiment are performed using the "Large-scale Atomic/Molecular Massively parallel Simulator" (LAMMPS) developed by Plimpton [11] and images were created using OVITO visualization software [12]. A cube of FCC aluminum with <100> orientation with rough dimensions of 100x100x100 Å^3 was prepared, using the lattice constant of Aluminum of 4.0495 Å. This sample was then put through an equilibration process to ensure a relaxed structure was achieved before indentation. First, the system was equilibrated to 300 K and 1 atm for 100 ps using a Nose-Hoover thermostat and barostat (NPT) with periodic boundary conditions. Next, the boundary conditions for the indentation direction were changed to fixed and equilibrated at 300 K, constant volume (NVT) for another 100 ps. Lastly, the bottom three layers of atoms were locked in place to prevent translational movement during the indentation procedure and the system was again equilibrated at 300 K, NVT for an additional 100 ps.

Indentation was performed using a rigid indenter to eliminate the force field of the indenter as a variable in this comparison work. The indentation procedure was displacement-controlled, meaning the indenter is lowered into the sample at a constant velocity. The indenter was lowered into the sample at 0.1 Å/ps (or 10 m/s) to a depth of 10 Å, then retracted at the same velocity. This rate is several magnitudes greater than an actual indentation test procedure and is a limitation of current computational resources. However, Ju et al. notes that indentation speeds below 80 m/s will have no effect on the predicted modulus [13]. This chosen speed is therefore well within the range for the indenter velocity to be negligible on the material properties. Further information on simulation parameters can be found in Table 1. The applied force of the indenter is calculated by:

$$F = -k(R - r)^2, r < R \tag{2.1}$$

$$F = 0, r > R \tag{2.2}$$

Where F is the applied force, R is the radius of the indenter, r is the distance from the center of the indenter to the atom and k is a force constant that describes the rigidity of the indenter. Essentially, if the indenter sphere and atoms overlap, the indenter will repel them away from its center. Overall, eight different force fields provided through the NIST Interatomic Potential Repository [14] were used to model the atomic interactions during the nanoindentation.

Table 2.1 – MD Simulation details for nanoindentation of an aluminum prism.

Simulation Parameter	Value
Simulation Timestep, dt	1 fs (0.5 fs for ReaxFF)
Ensemble	Nosé-Hoover Thermostat (NVT)
Temperature, T	10.0 K
Indenter Radius, R	50 Å
Indentation Velocity, v	10 m/s (0.1 Å/ps)
Force Constant, k	10.0 eV/Å^2
Indentation Depth, h	10.0 Å
Total Time	2*(10.0 Å)/(0.1 Å/ps) = 200 ps
Simulation Steps	(200 ps)*(0.001 ps/step) = 200,000 steps

2.2.1 Embedded-atom Method (EAM) and Modified EAM (MEAM) Potentials

The Embedded-atom method created by Daw and Baskes [15] is a popular force field choice for predicting bulk properties of metals. The method calculates the potential energy of the atom Ebased on its distance from other atoms, its embedding potential $F(\rho_i)$ and pair interaction potential $V(r_{ij})$ which describe how two atoms i and j form a favorable bond distance. The embedding potential is a function of the atoms' electron density $\phi\left(r_{ij}\right)$. EAM calculates bond energy and optimal difference as the sum of the forces of surrounding atoms, which makes it a many-body type force field. The energy is a function of the electron density function.

One of the shortcomings in EAM is it assumes the electron density functions surrounding each atom are spherical. For FCC metals this is a valid assumption but this makes it difficult for EAM to correctly model systems where direction and orientation are highly important. [16] The Modified EAM (MEAM) potential [17] better accounts for the bond angle between atoms, to allow it to be more accurate for certain stacking configurations like BCC and HCP materials.

The functions $F(\rho_i)$, $\phi(r_{ij})$ and $V(r_{ij})$ are fitted potentials, meaning they are created by tuning parameters to match empirical data created from ab-initio calculations. The choice of parameters is made based on the potential's intended application. This implies that different EAM potentials will have different simulation results based on how the parameters are fitted. Therefore, it is important to examine what applications were each potential built for. Table 2.2 shows the various potentials chosen for this simulation and their applications. A variety of available EAM and MEAM potentials were selected that are parameterized for both aluminum in its pure metal form and as an alloying agent.

$$E(r_{ij}) = \frac{1}{2}\sum_{ij} V(r_{ij}) + \sum_{i} F(\rho_i) \tag{2.3}$$

$$\rho_i = \sum_{i} \phi(r_{ij}) \tag{2.4}$$

2.2.2 ReaxFF Potential

The ReaxFF potential designed by Van Duin et al. is based a bond-order based method based on polarisable charges, making ReaxFF an accurate model for covalent, metal and electrostatic interactions [9,18]. This force field predicts the bond-order between two atoms based on their distance apart, which is used to determine the topology and energy shared. The system's energy is calculated by:

$$E_{system} = E_{bond} + E_{over} + E_{angle} + E_{tors} + E_{vdWaals} + E_{Coulomb} + E_{Specific} \quad (2.5)$$

Where E_{bond} is a function of the interatomic distance between atoms, E_{angle} and E_{tors} describe the energy associated with angle and torsional strain, $E_{vdWaals}$ and $E_{Coulomb}$ are the electrostatic interactions between atoms, E_{over} describes bond order energy considerations, and $E_{Specific}$ are for properties of interest of a given system[19]. Like EAM and MEAM, it is a multi-body potential and is useful for predicting yield and dislocations in metallic structures. The ReaxFF force fields and descriptions are shown in Table 2.2. While the Al data in these ReaxFF potentials were parameterized for single crystal Al, their applications use Al as part of a zeolite structure and catalyst surfaces.

Table 2.2 – Name and descriptions of force fields investigated.

EAM	**Description**
Al03 [20]	Lattice properties, vacancy energy, planar defects, surface energies
Al99 [21]	Elastic constants, vacancy formation energy, stacking fault energies, surface energies
MDSL [22]	Elastic constants, vacancy formation energy, elastic constants, melting points
NiAlH [23]	Elastic constants, vacancy formation energy, stacking fault energies, Al as an alloying agent
MEAM	
MgAlZn [24]	Lattice properties, elastic constants, surface energy, Al as an alloying agent
meamAlU [25]	Elastic constants, point defect properties, vacancy formation energy, pure Al
meamAl [25]	Elastic constants, point defect properties, vacancy formation energy, pure Al
ReaxFF	
SiAlOLi [26]	Lattice properties, heats of formation, elastic properties, pure metal and alloy properties
CaSiAlO [27]	Zeolite housing and particle shaping
AlH2O [28]	Heat of formation, surface energies, water adsorption
CHOAlSi [29]	Bond dissociation energies, heat of formation, Al as an alumino-silicate

2.3 Calculation of Young’s Modulus

Overall, there are two accepted techniques for measuring modulus from a nanoindentation curve: The Hertz approximation [30] and the Oliver & Pharr method (O&P) [31-32]. The former uses the initial elastic region of the indentation curve to extract modulus while the latter uses the slope of the unloading curve and projected contact area to calculate modulus and hardness. O&P is the preferred method for analyzing real-life nanoindentation experiments as it’s applicable to many indenter shapes. However, the Hertz method can still be useful for nanoindentation simulations with spherical indenters, when the indentation depth is small [33]. Therefore, both techniques were used to calculate an elastic modulus from the nanoindentation simulation and compared with experimental data.

2.3.1 Hertz Method

Figure 2.1 shows the indentation of a flat surface by a spherical indenter. The Hertz equation for force applied by this indenter is given by the following equation:

$$F = \frac{4}{3} E_r R^{0.5} h^{1.5} \tag{2.6}$$

Where F is the applied force, R is the radius of the indenter, δ is the indentation distance. The term E_r represents the reduced modulus of the system which describes the resistance to deformation by both the sample and the indenter. The reduced modulus is calculated by:

$$E_r = \left[\frac{1 - v_i^2}{E_i} + \frac{1 - v_s^2}{E_s}\right]^{-1} \tag{2.7}$$

Where v_i, E_i, v_s and E_s are the Poisson's ratio and Young's Modulus for the indenter and sample respectively. In this simulation, the indenter is considered perfectly rigid so E_s will equal infinity. The equation will therefore reduce to:

$$E_r = \frac{E_s}{1 - v_s^2} \tag{2.8}$$

The Hertz model works under the assumption of small indentation depths relative to the indenter's diameter. The Hertz model is compared to the first 5 Å of the simulation's force-displacement curve and modulus is calculated using regression analysis.

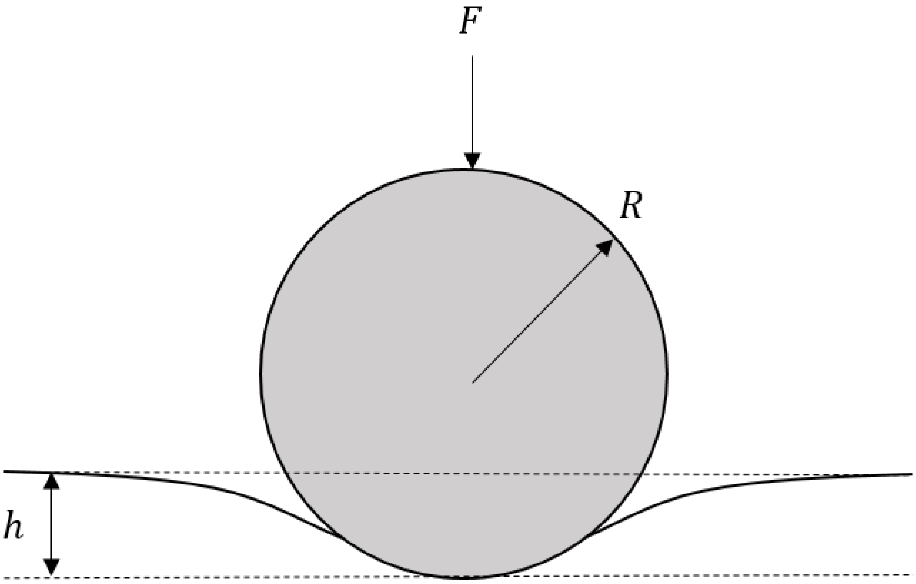

Figure 2.1 – Diagram of a spherical indenter indenting a flat surface.

2.3.2 Oliver-Pharr Method

The Oliver & Pharr (O&P) method expresses the elastic modulus of the indented sample as:

$$E_r = \frac{\sqrt{\pi}}{2} * \frac{S}{\sqrt{A_c}} \tag{2.9}$$

Where S is the slope of the unloading curve at its maximum displacement, and A_c is the projected contact area of the indenter at maximum displacement.

Figure 2.2 and Figure 2.3 show a sample indentation loading curve and indenter geometry respectively to illustrate these variables. The unloading curve is estimated using the following power law equation:

$$F = c\left(h - h_f\right)^m \tag{2.10}$$

Where h_f is the final indentation depth of the sample after the indenter is removed, and c and m are coefficients determined by fitting the equation to the unloading curve. In real-life experiments, the exponent m is related to the indenter geometry and is typically between 1.0 and 2.0. For a spherical indenter with a small indent, the theoretical value of m is 1.5 [31]. Once these coefficients are determined, S is calculated by taking the first derivative of equation 2.10:

$$\left.\frac{dF}{dh}\right|_{h_{max}} = S = mc\left(h_{max} - h_f\right)^{m-1} \tag{2.11}$$

The final variable needed, contact area, is assumed as the projected area of the indenter at the sample's surface at maximum displacement as depicted in Figure 2.3. For a spherical indenter this is calculated as:

$$A_c = \pi a^2 \tag{2.12}$$

Where a is the projected contact radius at the sample's surface calculated by:

$$a = \sqrt{2Rh - h^2} \tag{2.13}$$

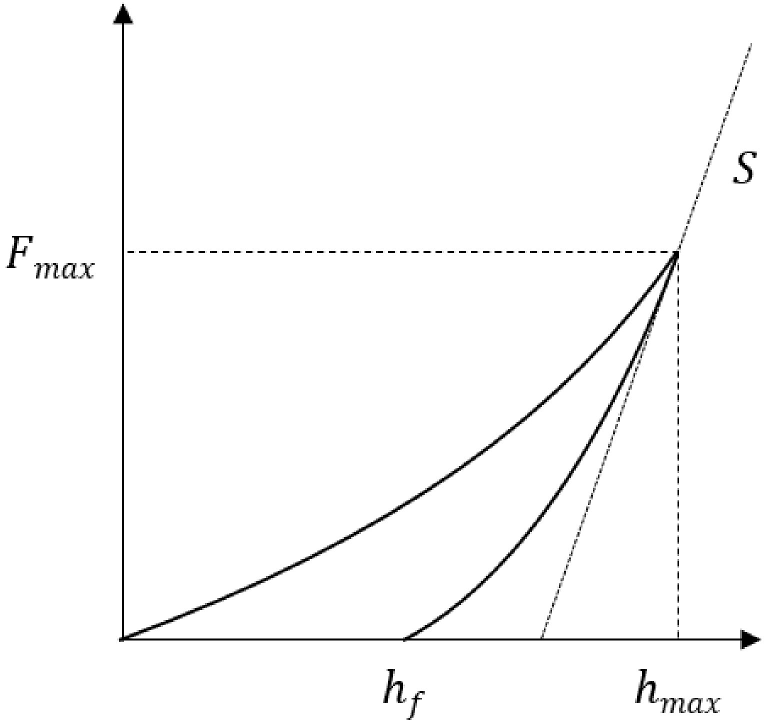

Figure 2.2 – Force-displacement curve showing the measurement of elastic modulus using the Oliver-Pharr method.

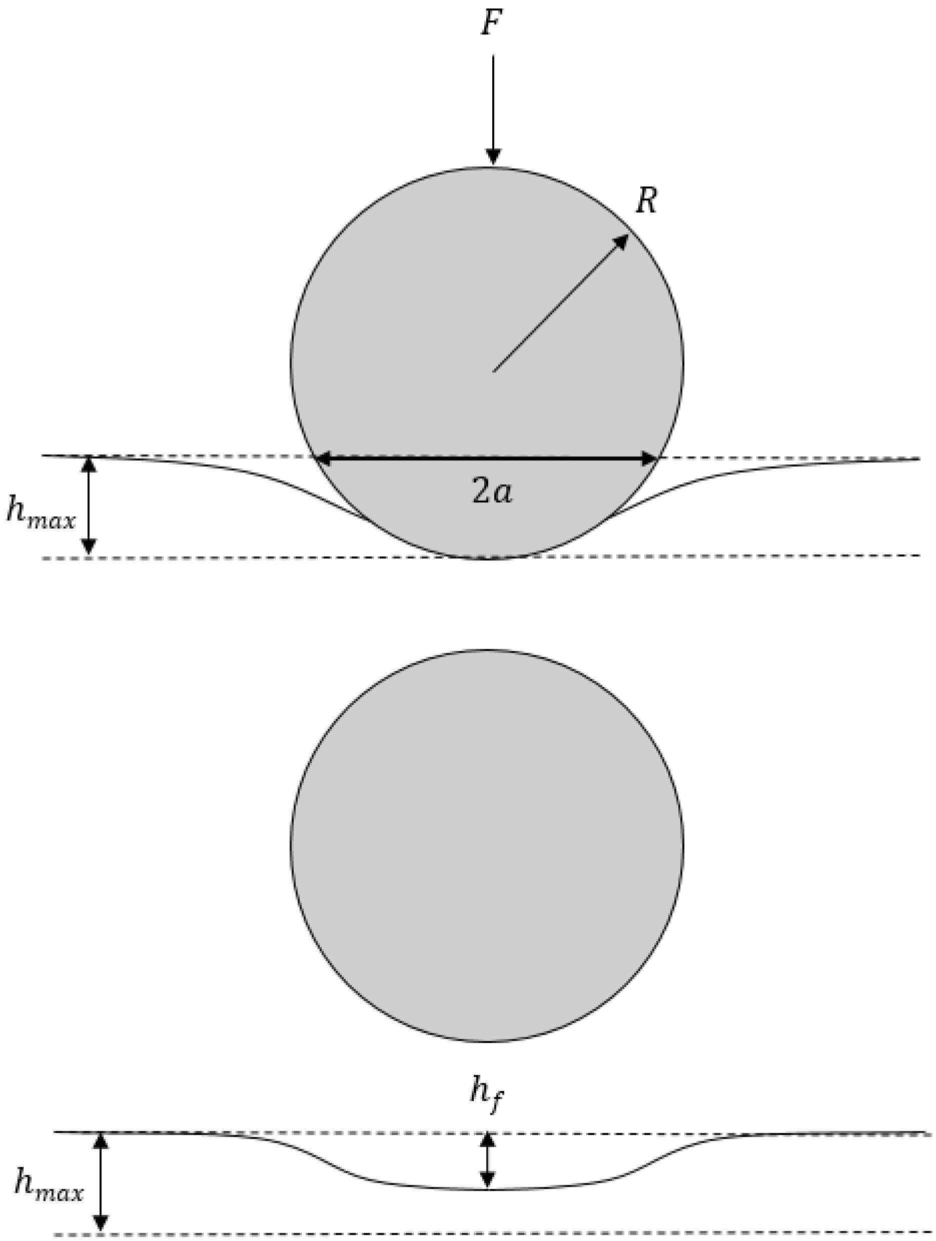

Figure 2.3 – Indentation geometry at max displacement and post loading.

2.4 Results and Discussion

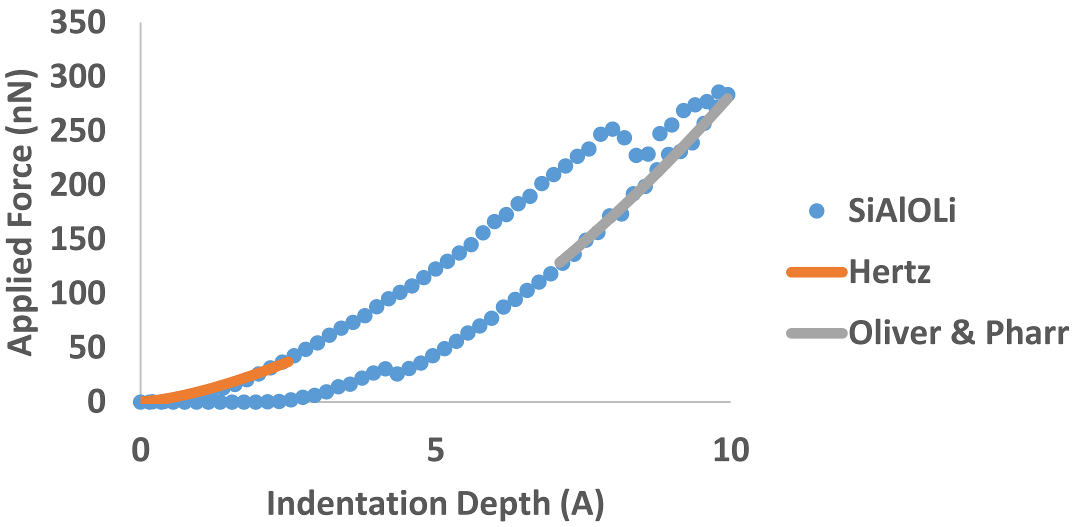

Figure 2.4 – Nanoindentation curve using the SiAlOLi ReaxFF force field with approximation curves highlighted.

After conducting each nanoindentation test (as described above), the resulting force-displacement curves were then used to compute mechanical properties and compare the relative accuracy of each force field. For example Figure 2.4 shows a simulated force-displacement curve using the ReaxFF type force field developed by Narayanan [26] and illustrates how modulus is extracted from the simulation data. The curve exhibits elastic behavior initially as it closely follows the Hertz approximation. In the latter half of the loading curve, the applied force begins to decrease as indentation depth increases. This represents the beginning of plastic deformation. To extract modulus accurately, the Hertz equation to be fitted to the loading curve prior to this occurrence. For consistency, all moduli calculated using the Hertz approximation were fitted to the first 2.5 Å of their system’s respective loading curves.

After reaching maximum indentation, the indenter is retracted at the same speed. During unloading the reaction force on the indenter is considered purely elastic deformation. The force continues to decrease as the indenter is lifted. The height at which the force hits zero represents the depth of the permanent dent made into the sample. The first 3 Å of the unloading curve are fitted to equation 2.10 using regression analysis to determine the modulus from the O&P method.

Figure 2.5 illustrates the sample before indentation, at full loading, and permanently dented after full retraction. The results for predicted elastic modulus for different force fields tested using both the Hertz and O&P methods are tabulated in Table 2.3 and are compared to the experimental modulus of 63.4 GPa for single crystal aluminum in the <100> direction [34]. Further, the resulting load-displacement curves are shown in Figure 2.6-

Figure 2.8. Overall, the results for each force field produced loading curves that closely followed the Hertz approximation initially, then underwent plastic deformation. Moreover, upon unloading, the curves were in good agreement with their respective power law approximations. The average value of the power law coefficient m as seen in equation 2.10 was 1.65, which is within the expect range and in fair agreement with the theoretical value of 1.5 for spherical indenters.

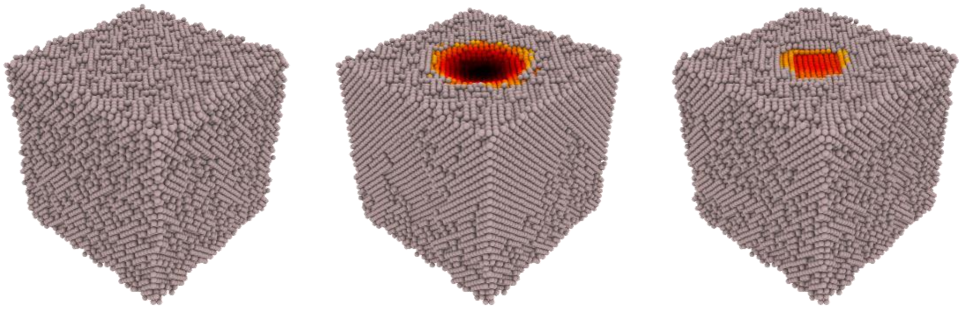

Figure 2.5 - Images of sample throughout nanoindentation process. The left image is the sample pre-indentation. Center image shows indenter at maximum depth, and right image shows the permanent imprint left in sample after the indenter is removed.

Table 2.3 – Elastic Modulus calculated by Hertz and O&P methods compared to experimental nanoindentation data of single crystal <1 0 0> aluminum.

	Pharr		**Hertz**	
Force Field	**Modulus (GPa)**	**% Error**	**Modulus (GPa)**	**% Error**
Al99	72	13	57	-11
Al03	71	11	45	-29
MDSL	66	4	46	-28
NiAlH	41	-36	34	-47
meamAl	84	32	49	-23
meamAlU	88	38	43	-32
AlZnMg	99	55	39	-39
CaSiAlO	81	27	80	26
SiAlOLi	90	41	86	35
AlH2O	80	26	87	37
CHOAlSi	84	32	81	27

2.4.1 EAM potentials

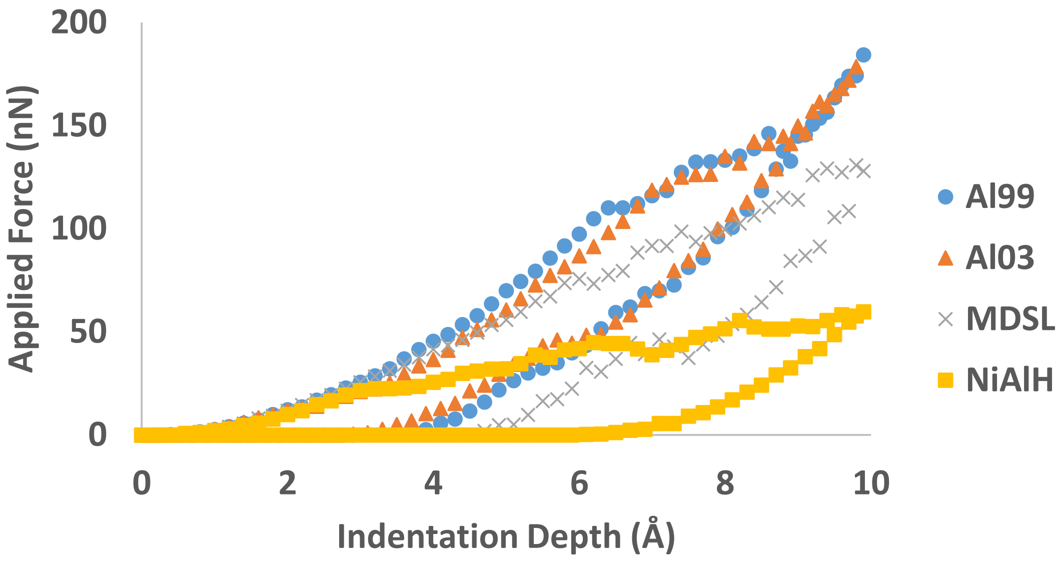

Figure 2.6 – Load-displacement curves for the Al99, Al03, MDSL and NiAlH EAM potentials.

The loading and unloading curves for the four EAM force fields are presented in Figure 2.6. The potentials are compared against the experimental modulus. The potentials moderately under-predicted the elastic modulus using the Hertz approximation while the O&P were in good agreement with the literature. Overall the O&P method more accurately calculated the modulus.

When attempting to explain the accuracy of each potential it is important to consider the purpose of development and the data used for parameterization. First, the Al03 [20], Al99 [21] and MDSL [22] potentials were created to match known data of aluminum's elastic constants and vacancy formation energies as well as parameterized against ab-initio calculations. Therefore, these potentials were developed with the specific purpose of describing Al-Al interactions and aluminum specific elastic properties. In contrast, the

NiAlH [23] was created to study the dislocation energies of Ni-Al alloys in the presence of hydrogen. All other force fields were created with elastic constants and dislocation structures in mind. Unlike the other three EAM potentials, this one in particular was not developed or parameterized against Al specific elastic data, and, despite being listed as an aluminum potential, was not developed to specifically describe single crystal aluminum. Therefore, this highlights the importance of considering potential development and likely explains the simulations' relative accuracy compared to the experimental.

2.4.2 MEAM potentials

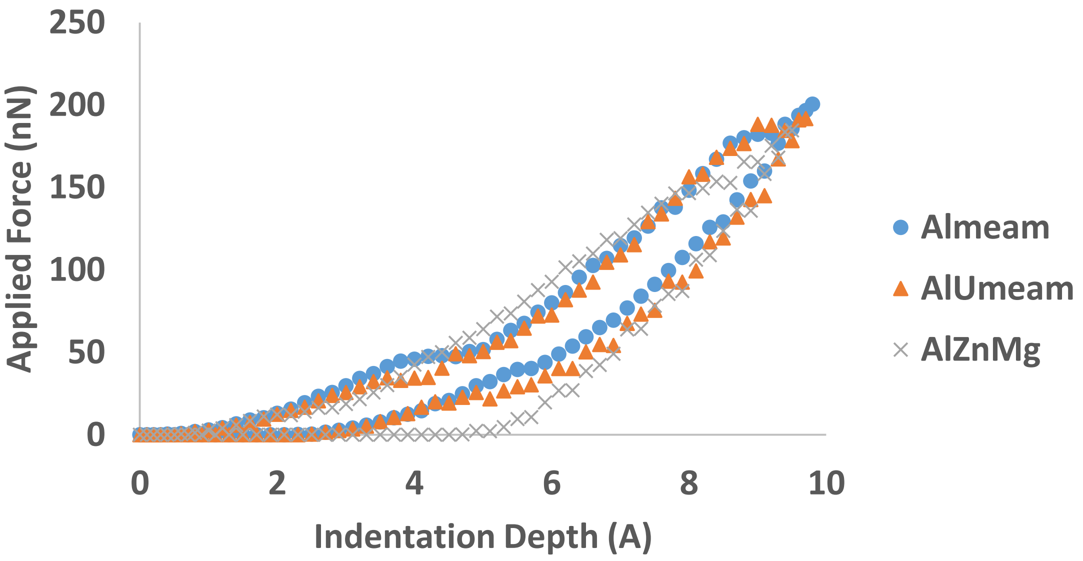

Figure 2.7 – Load-displacement curves for AlZnMg, Al.meam and AlU.meam MEAM potentials.

The MEAM potentials performed poorly in predicting modulus. Like EAM, the three force fields under-predicted the modulus using the Hertz approximation. Using the O&P method, the predicted moduli were largely overestimated. The three load-displacement curves are the expected shape, but interestingly their loading curves are much smoother compared to the erratic drops in force found in the EAM curves. This implies there was much less plastic deformation observed in the MEAM force fields.

The potentials meamAl and meamAlU [25] were both optimized for measuring point defect properties of Al and Al-U systems for a large range of temperatures. The elastic constants of these force fields were found to be overestimated during parameterization, which may explain the large modulus obtained from the unloading curve. The AlZnMg [24] force field was parameterized against thermal, structural and elastic properties. The data for aluminum used in this force field however was created as an alloying agent for Mg-Al systems, not single crystal Al. This could explain why the modulus measurements were erroneous, even though it was fitted specifically to elastic data. This shows that of the MEAM force fields available through the NIST repository are parameterized suitably for modelling nanoindentation.

2.4.3 ReaxFF Potentials

The ReaxFF potentials also did not compare well with the literature modulus. All four force fields obtained similar moduli from both the Hertz and O&P models, all significantly overestimating. The most notable part of these force-displacement plots were their minimal drop in force during unloading compared to the other force field types. This indicates the models had very minimal plastic deformation during the 10 Å indentation. Upon unloading, the force decrease of each potential happens at rates very similar to their respective loading curves. This is in contrast to the EAM and MEAM potentials where their initial unloading slopes are relatively large. Furthermore, the final indentation depth h_f for the ReaxFF simulations were the smallest compared to the other two methods. All of these observations show that not only did the ReaxFF force fields poorly predict the modulus, they are also shown to be unsuitable in modelling plastic response in single crystal Al. A possible reason for these results can be seen by the parametrization used to make these potentials. Presently there are no ReaxFF forcefields available that focus solely on the mechanical properties of single crystal Al. While the SiAlOLi was used to simulate elastic properties and parameterized for bulk Al, it was intended for testing for Li-Al silicate ceramics. Similarly, the CaSiAlO force field was made for zeolite compounds which are aluminosilicate minerals, CHOAlSi was intended for modelling hydrocarbon combustion on Al-Si catalysts and Al-H2O was made for modeling water adsorption on metal surfaces.

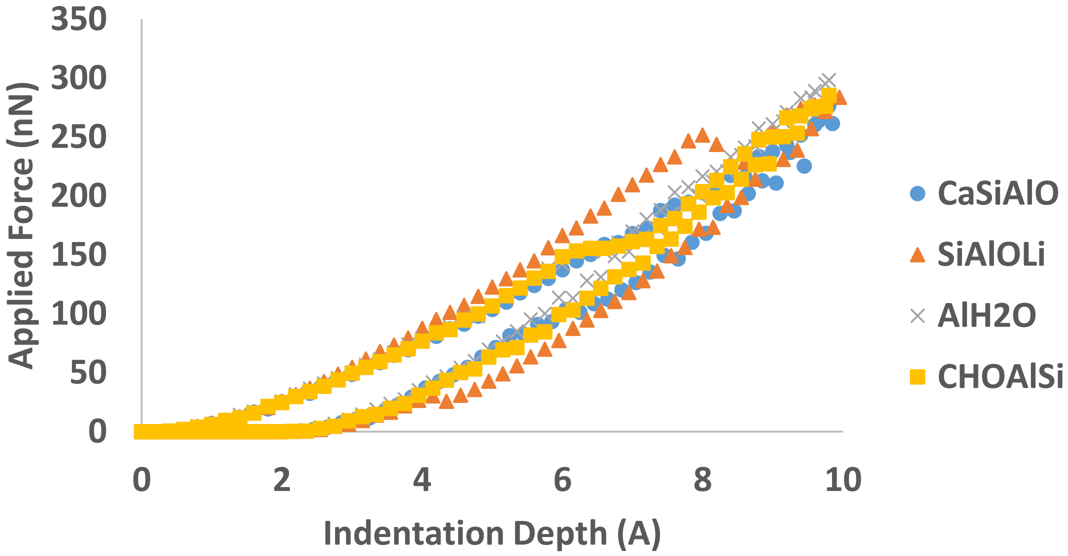

Figure 2.8 – Load-displacement curves for SiAlOLi and CaSiAlO ReaxFF potentials.

2.5 Conclusions

Molecular Dynamics offers a new method of testing the mechanical properties of engineering materials. In order to achieve realistic results from these simulations, it is essential to choose a force field potential appropriate for the application. The nanoindentation simulations showed good agreement with experimental data for EAM type force fields, while the MEAM and ReaxFF type potentials had significant error. This can be attributed to the fact that the available EAM force fields are better parameterized for elastic properties and yield behavior, while the MEAM potentials selected were more focused on crystal structure and Al as an alloying agent. Further, the ReaxFF force fields were designed for aluminosilicates and as catalysts for hydrocarbon interactions. The elastic modulus results from using the Hertz and O&P methods were also compared. For EAM and MEAM, the Hertz method consistently underestimated the modulus while the O&P method overestimated. For ReaxFF, both methods of calculation gave similar results. Therefore, of the three force-fields presented in this study, EAM is the recommended choice of potential for examining nanoindentation in aluminum and O&P is the best method for calculating modulus for aluminum. This work demonstrates the importance of choosing potentials parameterized for its intended purpose. Moreover, future work should investigate developing potentials specifically for the purpose of simulating nanoindentation.

References

[1] J. Li *et al*, "Diffusive molecular dynamics and its application to nanoindentation and sintering," *Physical Review B,* vol. 84, *(5),* pp. 054103, 2011.

[2] T. Fang and J. Wu, "Molecular dynamics simulations on nanoindentation mechanisms of multilayered films," *Computational Materials Science,* vol. 43, *(4),* pp. 785-790, 2008.

[3] C. J. Ruestes, I. Alhafez and H. M. Urbassek, "Atomistic Studies of Nanoindentation: A Review of Recent Advances," *Crystals,* vol. 7, *(10),* 2017. . DOI: 10.3390/cryst7100293.

[4] E. T. Lilleodden *et al*, "Atomistic simulations of elastic deformation and dislocation nucleation during nanoindentation," *J. Mech. Phys. Solids,* vol. 51, *(5),* pp. 901-920, 2003. . DOI: 10.1016/S0022-5096(02)00119-9.

[5] D. Christopher, R. Smith and A. Richter, "Atomistic modelling of nanoindentation in iron and silver," *Nanotechnology,* vol. 12, *(3),* pp. 372-383, 2001. . DOI: 10.1088/0957-4484/12/3/328.

[6] J. A. Stewart and D. E. Spearot, "Atomistic simulations of nanoindentation on the basal plane of crystalline molybdenum disulfide (mos 2)," *Atomistic Simulations of Nanoindentation on the Basal Plane of Crystalline Molybdenum Disulfide (MoS2),* vol. 21, *(4),* pp. 045003, 2013. . DOI: 10.1088/0965-0393/21/4/045003.

[7] A. K. Nair *et al*, "Nanoindentation of thin films: Simulations and experiments," *J. Mater. Res.,* vol. 24, *(3),* pp. 1135-1141, 2009. . DOI: 10.1557/jmr.2009.0136.

[8] S. Goel *et al*, "Designing nanoindentation simulation studies by appropriate indenter choices: Case study on single crystal tungsten," *Computational Materials Science; Computational Materials Science,* vol. 152, pp. 196-210, 2018. . DOI: 10.1016/j.commatsci.2018.04.044.

[9] M. Yaghoobi and G. Z. Voyiadjis, "Effect of boundary conditions on the MD simulation of nanoindentation," *Computational Materials Science,* vol. 95, pp. 626-636, 2014. . DOI: 10.1016/j.commatsci.2014.08.013.

[10] S. Rassoulinejad-Mousavi, Y. Mao and Y. Zhang, "Evaluation of copper, aluminum, and nickel interatomic potentials on predicting the elastic properties," *J. Appl. Phys.,* vol. 119, *(24),* 2016. . DOI: 10.1063/1.4953676.

[11] S. Plimpton, "Fast Parallel Algorithms for Short- Range Molecular Dynamics," *Journal of Computational Physics,* vol. 117, *(1),* pp. 1-19, 1995. . DOI: 10.1006/jcph.1995.1039.

[12] A. Stukowski, "Visualization and analysis of atomistic simulation data with OVITO–the Open Visualization Tool," *Modell Simul Mater Sci Eng,* vol. 18, *(1),* pp. 015012, 2009.

[13] S. -. Ju *et al*, "The nanoindentation responses of nickel surfaces with different crystal orientations," *Molecular Simulation,* vol. 33, *(11),* pp. 905-917, 2007. DOI: 10.1080/08927020701392954.

[14] C. A. Becker *et al*, "Considerations for choosing and using force fields and interatomic potentials in materials science and engineering," *Current Opinion in Solid State and Materials Science,* vol. 17, *(6),* pp. 277-283, 2013. . DOI: https://doi.org/10.1016/j.cossms.2013.10.001.

[15] M. S. Daw and M. I. Baskes, "Embedded- atom method: Derivation and application to impurities, surfaces, and other defects in metals," *Physical Review B,* vol. 29, *(12),* pp. 6443-6453, 1984. . DOI: 10.1103/PhysRevB.29.6443.

[16] M. A. Tschopp, D. E. Spearot and D. L. McDowell, "Chapter 82 - influence of grain boundary structure on dislocation nucleation in FCC metals," in *Dislocations in Solids,* J. P. Hirth, Ed. 2008, Available: http://www.sciencedirect.com/science/article/pii/S1572485907000022. DOI: https://doi.org/10.1016/S1572-4859(07)00002-2.

[17] M. I. Baskes *et al*, "Second nearest- neighbor modified embedded atom method potentials for bcc transition metals," *Physical Review B - Condensed Matter and Materials Physics,* vol. 64, *(18),* pp. , 2001. . DOI: 10.1103/PhysRevB.64.184102.

[18] A. C. T. Van Duin *et al*, "ReaxFF: A reactive force field for hydrocarbons," *Journal of Physical Chemistry A,* vol. 105, *(41),* pp. 9396-9409, 2001. . DOI: 10.1021/jp004368u.

[19] T. P. Senftle *et al*, "The ReaxFF reactive force- field : development, applications and future directions," *Npj Computational Materials,* vol. 2, *(1),* 2016. . DOI: 10.1038/npjcompumats.2015.11.

[20] R. Zope and Y. Mishin, "Interatomic potentials for atomistic simulations of the Ti-Al system," *Physical Review B; Phys.Rev.B,* vol. 68, *(2),* 2003. . DOI: 10.1103/PhysRevB.68.024102.

[21] Y. Mishin *et al*, "Interatomic potentials for monoatomic metals from experimental data and ab initio calculations," *Physical Review B; Phys.Rev.B,* vol. 59, *(5),* pp. 3393-3407, 1999. . DOI: 10.1103/PhysRevB.59.3393.

[22] J. B. Sturgeon and B. B. Laird, "Adjusting the melting point of a model system via Gibbs-Duhem integration: Application to a model of aluminum," *Physical Review B - Condensed Matter and Materials Physics,* vol. 62, *(22),* pp. 14720-14727, 2000. . DOI: 10.1103/PhysRevB.62.14720.

[23] E. A. J, "Trapping of hydrogen to lattice defects in nickel," *Modell Simul Mater Sci Eng,* vol. 3, *(3),* pp. 289-307, 1995. . DOI: 10.1088/0965-0393/3/3/001.

[24] D. E. Dickel *et al*, "New interatomic potential for mg– al– zn alloys with specific application to dilute mg- based alloys," *Modelling and Simulation in Materials Science and Engineering,* vol. 26, *(4),* pp. 045010, 2018. . DOI: 10.1088/1361-651X/aabaad.

[25] M. I. Pascuet and J. R. Fernández, "Atomic interaction of the MEAM type for the study of intermetallics in the Al– U alloy," *J. Nucl. Mater.,* vol. 467, pp. 229-239, 2015. . DOI: 10.1016/j.jnucmat.2015.09.030.

[26] B. Narayanan *et al*, "A reactive force field for lithium- aluminum silicates with applications to eucryptite phases," *Modell Simul Mater Sci Eng,* vol. 20, *(1),* 2012. . DOI: 10.1088/0965-0393/20/1/015002.

[27] M. C. Pitman and A. van Duin, "Dynamics of Confined Reactive Water in Smectite Clay- Zeolite Composites," *J. Am. Chem. Soc.,* vol. 134, *(6),* pp. 3042-3053, 2012. . DOI: 10.1021/ja208894m.

[28] M. F. Russo *et al*, "Molecular dynamic simulation of aluminum–water reactions using the ReaxFF reactive force field," *International Journal of Hydrogen Energy,* vol. 36, *(10),* pp. 5828-5835, 2011. . DOI: https://doi.org/10.1016/j.ijhydene.2011.02.035.

[29] F. Castro-Marcano and A. C. T. van Duin, "Comparison of thermal and catalytic cracking of 1-heptene from ReaxFF reactive molecular dynamics simulations," *Combustion and Flame,* vol. 160, *(4),* pp. 766-775, 2013. . DOI: https://doi.org/10.1016/j.combustflame.2012.12.007.

[30] K. Johnson, "Contact Mechanics," *Proceedings of the Institution of Mechanical Engineers Part J-Journal of En; Proc.Inst.Mech.Eng.Part J.-J.Eng.Tribol.,* vol. 223, pp. 254-254, 2009.

[31] W. C. Oliver and G. M. Pharr, "Measurement of hardness and elastic modulus by instrumented indentation: Advances in understanding and refinements to methodology," *J. Mater. Res.,* vol. 19, *(1),* pp. 3-20, 2004. . DOI: 10.1557/jmr.2004.19.1.3.

[32] W. C. Oliver, "An improved technique for determining hardness and elastic modulus using load and displacement sensing indentation experiments," *J. Mater. Res.*, vol. 7, *(6)*, 1992.

[33] E. K. Njeim and D. F. Bahr, "Atomistic simulations of nanoindentation in the presence of vacancies," *Scripta Materialia*, vol. 62, *(8)*, pp. 598-601, 2010. . DOI: https://doi.org/10.1016/j.scriptamat.2010.01.006.

[34] G. N. Kamm and G. A. Alers, "Low Temperature Elastic Moduli of Aluminum," *J. Appl. Phys.*, vol. 35, *(2)*, pp. 327-330, 1964. Available: https://doi.org/10.1063/1.1713309. DOI: 10.1063/1.1713309.

3. Molecular Dynamics Study on the Mechanical Properties of the DGEBA/DETDA Polymer System

Abstract: Epoxy resins include a vast range of structural materials used in many industries, and much research focuses on improving their mechanical, thermal and electrical properties for a wide collection of applications. As all properties are inherently a function of the polymer's molecular structure, Molecular Dynamics (MD) is an intriguing field for examining the effect of bonding and topology on an epoxy's performance. In this work an epoxy network consisting of Bisphenol A diglycidyl ether (DGEBA) and Diethyltoluenediamine (DETDA) is constructed using LAMMPS molecular modelling software and its mechanical properties are tested by means of a tensile test. The same DGEBA/DETDA polymer was created and tested experimentally to compare to the simulation results. Dog-bone specimens were machined and underwent tensile testing following the ASTM D638-14 standard. The simulations were found to be in good agreement with the experimentally tested samples for Young's Modulus and Poisson's Ratio. They were also found to slightly overestimate the density. The MD simulations showed the expected trend of increasing modulus and density as the degree of cure increased. This work also highlights a refined method for simulating crosslinking/curing of the epoxy samples, leading to less computational time and more accurate modelling.

Note: This paper is currently in preparation for submission. Ref: Pratt, D.R., Elruby, A.Y., and Nakhla, S., "Molecular Dynamics Study on the Mechanical Properties of the DGEBA/DETDA Polymer System", (in Preperation).

3.1 Introduction

Epoxy polymers are an expansive area of material composites used throughout major industries like aerospace, structural and medicine. These composite materials are known for their appealing thermomechanical properties and light weight. Particularly, epoxy polymers have excellent flexural strength, corrosion resistance, good adhesion to metal surfaces and resistance to thermal wear [1]. These characteristics give epoxies many applications as coatings, electronic insulation, adhesives and structural use [2]. There are two major components to an epoxy polymer: the epoxy resin and the curing agent. Of the available epoxy resins, bisphenol A is by far the most popular one used commercially. This is due to its low-cost production, its relatively low melting point making it easy to mold and because it doesn't require a high degree of purity needed in other polycarbonate resins [3]. Epoxy resins are very versatile and works with many different curing agent types. Amine-based curing agents in particular are widely used in industry because of their desirable properties and their high reactivity with epoxy resins [4].

Chemically, epoxy structures are created by reacting the resin and curing agent molecules to form the coalesced polymer material in a process called crosslinking. The epoxy resin gets its name from the epoxide ring functional group found in the molecule. This serves as the reaction site for the crosslinking reaction. The amine of the hardener reacts with the epoxide ring to form a covalent bond between the two monomers. This reaction happens multiple times on each molecule to form the thermoset, crosslinked polymer network. There are many different types of amine curing agents used which give the polymer different degrees of crosslinking as well as influence the composite's material properties. Commonly used amine curing agents include diethylene triamine (DETA), triethylenetetramine (TETA) and diethyltoluenediamine (DETDA). Other considerations made for choosing a curing agent include pot life, toxicity and curing temperature [4].

Molecular dynamic (MD) simulations have become a very lucrative field for modeling epoxy resin systems. An epoxy's performance is very dependent on the chemical and bonding structure of its monomers, yet manufacturing and testing for these properties is both difficult and expensive [5]. The crosslinking density of a polymer is an extremely important aspect of a polymer. Many of the thermomechanical properties desired from epoxies are a function of this parameter including Young's modulus, shear modulus, yield strength, density and the glass transition temperature [6]. Crosslinking density is a percentage value of crosslinking reactions that occurred to the total crosslinking reactions possible. Many researchers use estimations to determine crosslink density based on the molecular weight of the resin monomers and the density of the material [7]. Another common method is through spectroscopic techniques such as Infrared (IR) to estimate the degree of curing. As such, much research has focused on using MD simulations to model, crosslink and predict mechanical properties of epoxy systems based on their bonding [8]. For instance, the work done by Fu et al. [9] used MD to simulate and compare the thermomechanical properties of the Bisphenol A diglycidyl ether (DGEBA) epoxy cured with different anhydride hardeners. The simulations were able to predict changes in density and modulus as a function of the monomers' topology. In another publication, Bandyopadhyay et al. [10] made MD simulations to track the crosslinking density of epoxy polymers and presented the effect of the degree of cure on density, modulus and glass transition temperature. More so, as epoxy resins are combined with other material structures, a full description of the chemical bonding between these two materials will be essential to understanding and predicting their adhesion and mechanical properties. For instance, simulations performed by Radue et al. [11] focused on the adhesion between the molecules of carbon nanotubes and an epoxy resin. Their work shows the epoxy resin structure has significant effects on the bonding strength of the composite, an observation that would be impossible to make in a real experiment.

In the pursuit of making more realistic and accurate models for epoxy systems, the goal of this work is to build a DGEBA/DETDA epoxy polymer model and compare its mechanical properties to experimental values. To set this paper apart from other similar works, we showcase a new method to perform crosslinking reactions in MD simulations. Previous papers that design and analyze similar epoxy models all tend to use a multistep cross-linking procedure in order to create bonds and perform structure minimization in separate steps [5], [9], [12]-[14]. The process presented here allows bonding and minimization are able to occur simultaneously. This makes the crosslinking method better resemble an actual curing procedure as well as reduce the computational time required.

3.2 Epoxy Modelling and Procedure

The two monomers to be modelled in this simulation are the Bisphenol A diglycidyl ether (DGEBA) epoxy resin and the Diethyltoluenediamine (DETDA) hardener shown in Figure 3.1. The molecules are parameterized using the Consistent Valence Force Field (CVFF) force field potential. CVFF was chosen for being an established force field for modelling the structure of organic molecules and is a commonly used force field for simulating epoxies [15]. This potential uses ab-initio data to describe the energy interaction of organic molecules through bond length, bond angle, torsion, out-of-plane bending, partial charge and Lennard-Jones non-bonding interactions. All MD simulations were performed using the open-source Large-scale Atomic/Molecular Massively Parallel Simulator (LAMMPS) [16] and images provided in this report were created using OVITO visualization software [17]. Five systems of 200 DGEBA and 100 DETDA molecules were created and mixed over 100 ps with a timestep of 1 fs using a Nose-Hoover thermostat (NVT) at low density (0.14 g/mL). It is important to have multiple systems to capture the inherent variance to MD simulations of this small scale. To ensure each system was mixed differently, the initial temperature and atom velocities were randomly chosen between 600 – 1000 K, then cooled to 300 K over the time interval. After this initial mixing, each system was slowly compressed to 1.21 g/mL over 4 ns at 300 K with regular energy minimizations every 20 ps to ensure a relaxed system, similar to the mixing done by Radue [18].

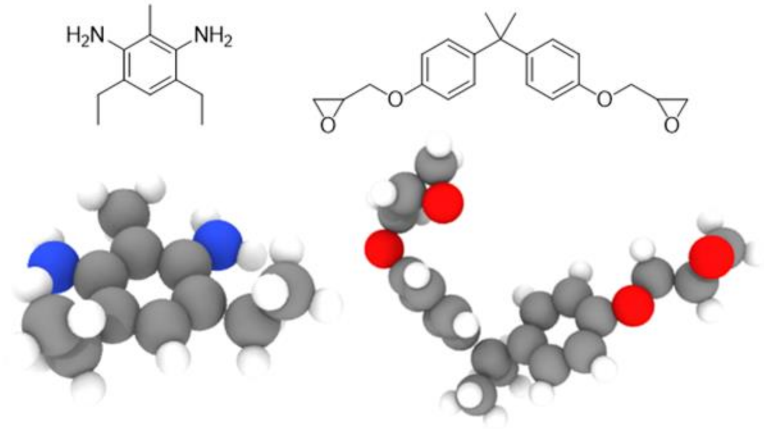

Figure 3.1 – Molecular structure of DGEBA and DETDA molecules.

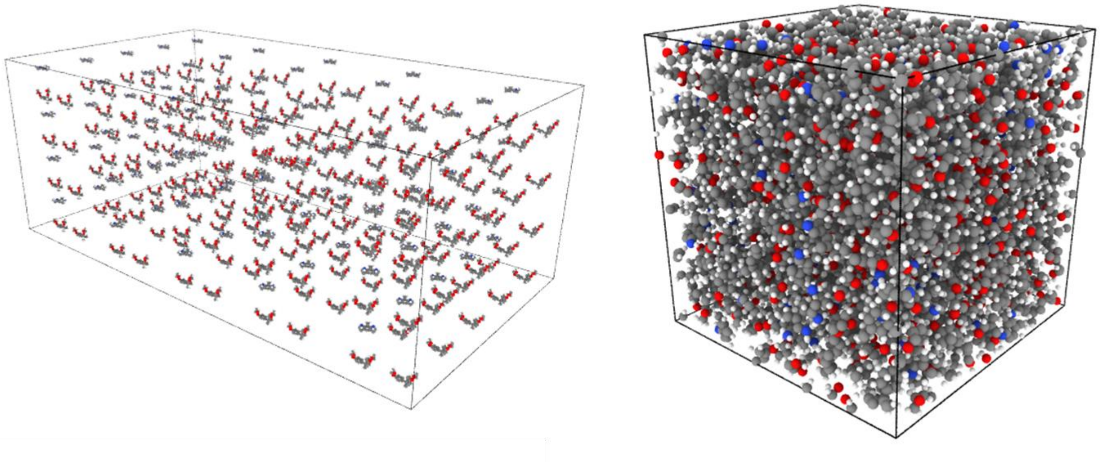

Figure 3.2 - Pre-mixing configuration of atoms (left) and the mixed, dense structure to be crosslinked.

The reaction to be simulated is the crosslinking epoxide opening reaction between the DGEBA and DETDA monomers as shown in

Figure 3.3. The nitrogen atom of the DETDA molecule can react with up to two epoxide rings from nearby DGEBA monomers and it is assumed that no other reactions occur. In this reaction, the nitrogen attacks the outer carbon which opens the epoxide ring. The negatively charged oxygen then forms a bond with one of the hydrogen atoms of the

nitrogen. Reactions occur in the simulation simply as a function of the distance between the DGEBA and DETDA monomers. That is, a cut-off radius is specified between the nitrogen atoms of DETDA and the terminal carbon of DGEBA's epoxide ring. When the two atoms are within this specified length, a reaction occurs and the surrounding atoms' topology (bonds, angles, dihedrals, etc) are updated to match the product. Reaction completion is measured by its crosslink density η calculated by:

$$\eta = \frac{N_{E-H}^{bonds}}{N_E f_E} \tag{3.1}$$

Where N_{E-H}^{bonds} is the number of crosslinking bonds formed between the epoxy and hardener monomers in the simulation, while N_E and f_E are the number of epoxy monomers present and number of bonds each epoxy molecule can form respectively [19]. For example, there are 200 epoxy monomers in this system which can each form two bonds so $N_E = 200$ and $f_E = 2$. If 154 crosslinking bonds formed, the crosslinking density would equal $\eta = 0.77$. The final crosslink density of a system during the curing process can be effectively controlled by increasing or decreasing the specified cut-off distance.

The monomer system crosslinking was performed using the "fix bond/react" command in LAMMPS, created by Gissinger et al. [20] This fix works by determining when the bonding atoms of DGEBA and DETDA are within a specific cut-off radius. If the atoms are within this distance, they will be 'reacted' together and their topology will be switched to match the product. "Fix bond/react" offers advantages over traditional crosslinking procedures used in the literature. In many publications, crosslinking needs to be broken up into two processes: bond-forming and post-bonding equilibration. This can be a very time-consuming process for large polymer systems. The script used in this procedure however allows several reactions and structure equilibration to happen simultaneously. When a crosslink reaction occurs, the atoms involved in the reaction are temporarily removed from the simulation's main thermostat and placed in a separate "fix nve/limit" system for 100 time steps (0.1 ps). This allows the atoms to quickly equilibrate from the initial, large spike in energy caused by crosslinking and eliminates the need for the crosslinking reaction to be halted for equilibrium. After this short timespan the atoms are released back in the system to further equilibrate as other reactions are occurring, allowing for a shorter and less resource intensive crosslinking procedure. It also better reflects an actual curing process where reactions and equilibration would of course happen together.

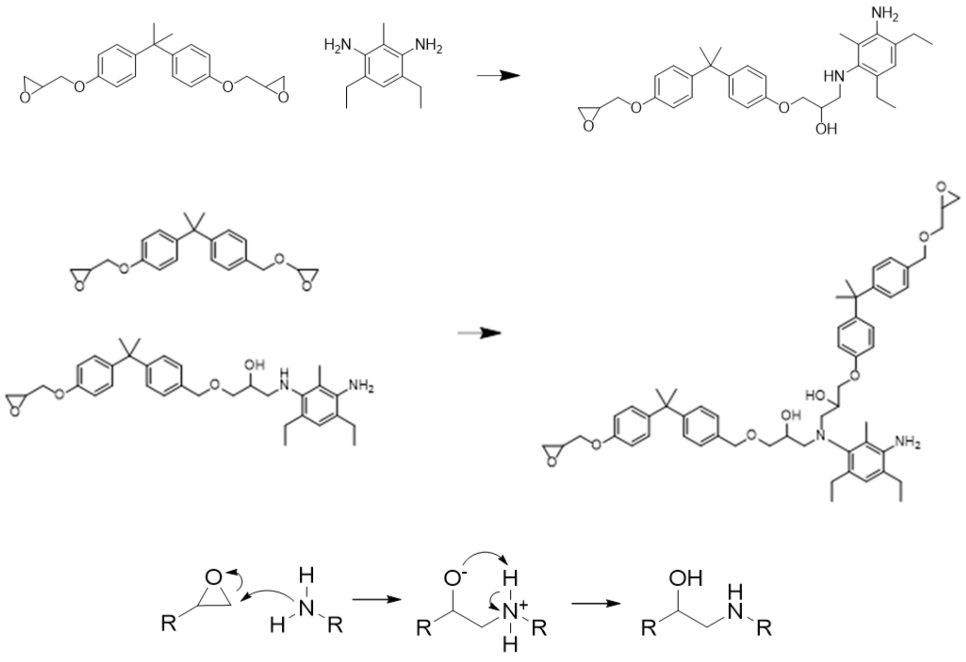

Figure 3.3 – Crosslinking reaction and reaction mechanism of DGEBA monomer crosslinking with DETDA.

Each system is initially crosslinked with a cut-off radius of 2.5 Å at 300 K for 300 ps. Then the radius is increased in increments of 0.5 Å and the system is allowed to further crosslink for the same time length or until the desired crosslink density is achieved. Figure 3.1 shows the effect of the cut-off radius on the degree of cure for each of the five samples. It is found that below 3 Å, no reactions are able to occur over the time length for any system. As the cut-off radius increases, the degree of curing increases the most rapidly between 3 to 5 Å. After 7.0 Å no more reactions occur, showing the systems have reached their maximum degree of curing possible. As the system approaches 100% crosslink density, the movement of atoms is heavily reduced due to steric hindrance of the cross-linked system. The maximum degree of curing achieved by the five samples are between 74-78%.

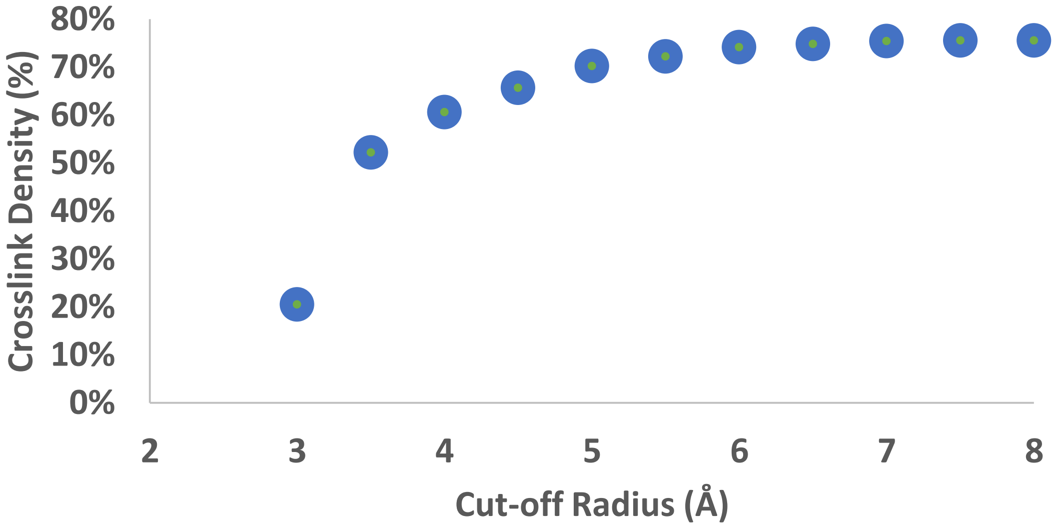

Figure 3.4 – The crosslink density achieved as a function of the crosslinking reaction cutoff radius.

After crosslinking, it is important to further equilibrate the polymer structure to remove residual stresses present. During the crosslinking simulation, bonds and angles can become stretched or compressed from their equilibrium lengths/angles which will impact the model's density and mechanical properties. In order to relax the polymer matrix, it needs to be slowly pressurized and decompressed through a series of NVT and NPT runs to allow the system to reorganize its chains to more optimal positions. In a process similar to the one done by Tam and Lau [15], the crosslinked system was pressurized from 0 to 50,000 atm then decompressed back to atmospheric pressure over 1 ns then put through for 5 ns in an NPT thermostat at 300 K and 1 atm to ensure the system had reached equilibrium. The density of the crosslinked system is determined by taking the average density over the final 2 ns of this process.

After equilibration the systems are put under uniaxial stress in the X-, Y- and Z-directions to determine Young's modulus and Poisson's ratio. The sample is stretched at a rate of 1e8 s^{-1} which is many magnitudes faster than an actual tension test. A faster strain rate is used because realistic speeds are not yet feasible due to computational limitations. The chosen velocity is commonly used in other works on tensile test simulations [18]. Pressure (and thus stress) is an inherently noisy value to measure in MD simulations on the scale of 10,000 atoms. To overcome this, stress values during straining are sampled using the fix ave/time command which calculates time averages during the test. In addition, every 0.1% strain the system is equilibrated for a short period of time (10 ps) to get a better sampling of the stress value. Each system is strained up to 3%.

3.3 Material and Mechanical Testing

The experimental testing was performed using the procedure for uni-axial tensile testing as performed by Elruby and Nakhla [21]. A slab of LAMPOXY61 Plain epoxy resin was prepared and cured for the current investigation by Polynt Composites Canada, Inc. The resin and hardener were mixed by a weight ratio 6:1 and allowed to cure in a metallic mold without vacuum application. This type of resin is commonly used in fiber-reinforced composites layup lamination. Table 3.1 shows the physical properties of the resin and hardener, as provided by the manufacturer.

Table 3.1. LAMPOXY61 physical properties at room temperature, 25ºC.

Lamination Epoxy properties	Resin material EPO-LAMPOXY 61	Hardener material EPO-LAMCAT 61
Viscosity (mPs)	1200-1400	25-50
Density (g/mL)	1.09-1.12	0.96-0.98
Weight (%)	85.72	14.28

To minimize surface flaws from both sides, the plain resin slab was milled down to a thickness of 9 mm. All six dog-bone tensile specimens were machined from the same epoxy slab as according to the ASTM D638-14 recommendations. The dimensions of these samples are shown below in Figure 3.5.

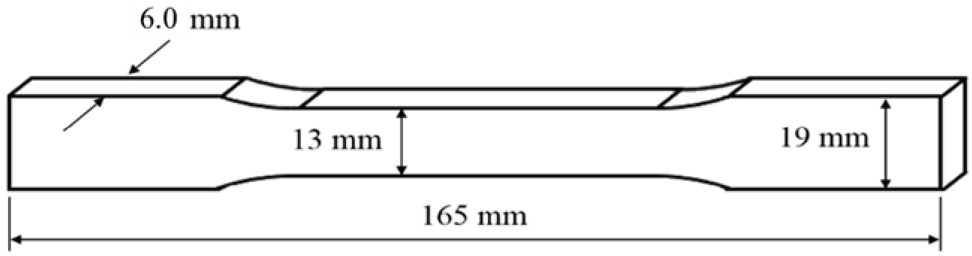

Figure 3.5 - Specimen geometry for ASTM D638-14 uniaxial tensile test.

Tension tests were carried out using the Instron E10000 load frame with a high precision non-contacting strain measurement (with a 0.5 microns ± 1.0 % resolution). The load frame showing the dog-bone specimen setup along with the video extensometer are shown in Figure 3.6. Specimens were fixed from their lower ends while a displacement load was applied to their upper end at a rate of 1 mm/min which is the minimum required by the testing standard. As can be seen from the zoomed view of dog-bone specimen, two longitudinal and lateral marks were used for local axial and lateral strain measurements, respectively. The specimens were marked within the specified standard gauge lengths for both strain measurements, axial and lateral.

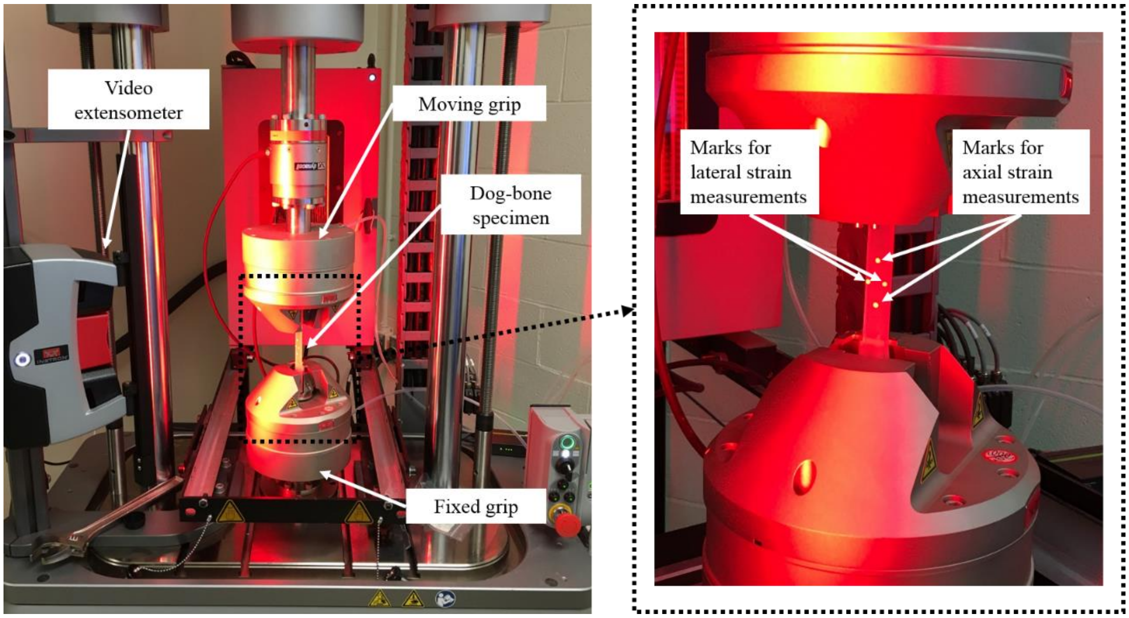

Figure 3.6 - Load frame setup showing video extensometer and dog-bone specimen marking.

Heavily cross-linked epoxy systems are known for their low strain to failure capacities which makes identifying the onset of yielding for such a material quite problematic. A novel approach for the accurate determination of yield onset is performing uniaxial testing procedures and synchronically video recording with strain measurements. Then, monochromic image analysis was used for efficient identification of yielding which observe stress-whitening caused by plastic deformation.

3.4 Uniaxial Tension Results

Figure 3.7 shows monochromic images from the synchronized record of a dog-bone specimen from testing. Plain epoxy resin has an opaque, transparent glass-like color (shown as pink in figure) which turns into an observable white color upon plastic deformation. The onset of plastic yield was found to begin at 226.3 s based on the monochromic image analysis. The inelastic deformation originated from mid-span and slightly biased towards the moving grip. Plastic deformation continued to build up throughout the specimen's narrow section which can be observed by inspecting the first and last time frames.

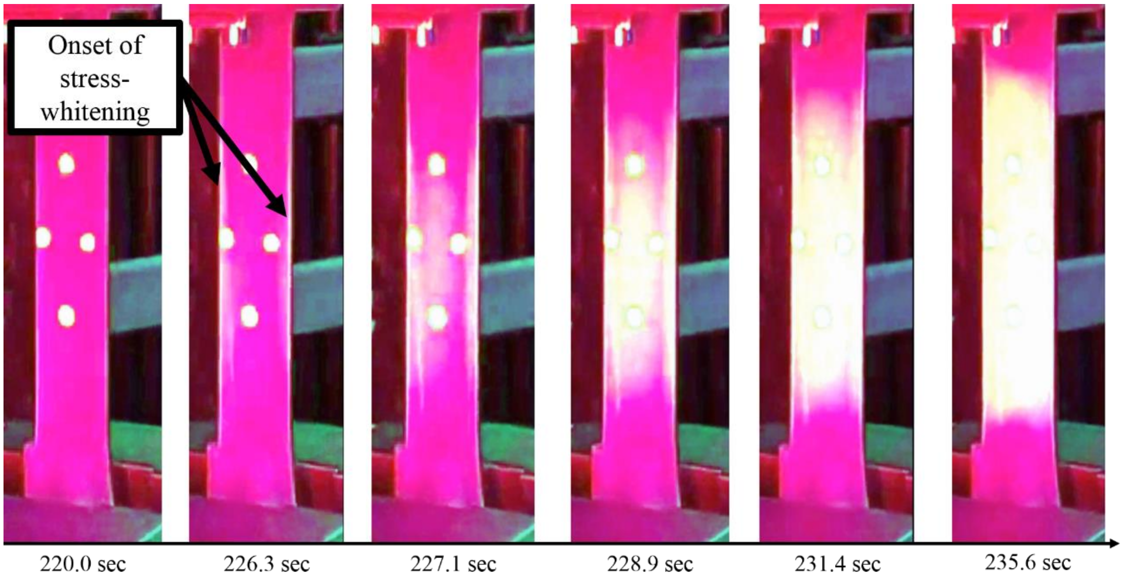

Figure 3.7 - Dog-bone specimen at different time frames showing stress whitening caused by inelastic deformation.

The stress-strain results of each dog-bone specimen are shown in Figure 3.8. Mechanical behaviors of all specimens are almost identical in the linear regime. Almost all specimens held a linear behavior up to 90% of the loading capacity followed by brittle failure. It is noteworthy to mention that none of the specimens showed a necking type of failure.

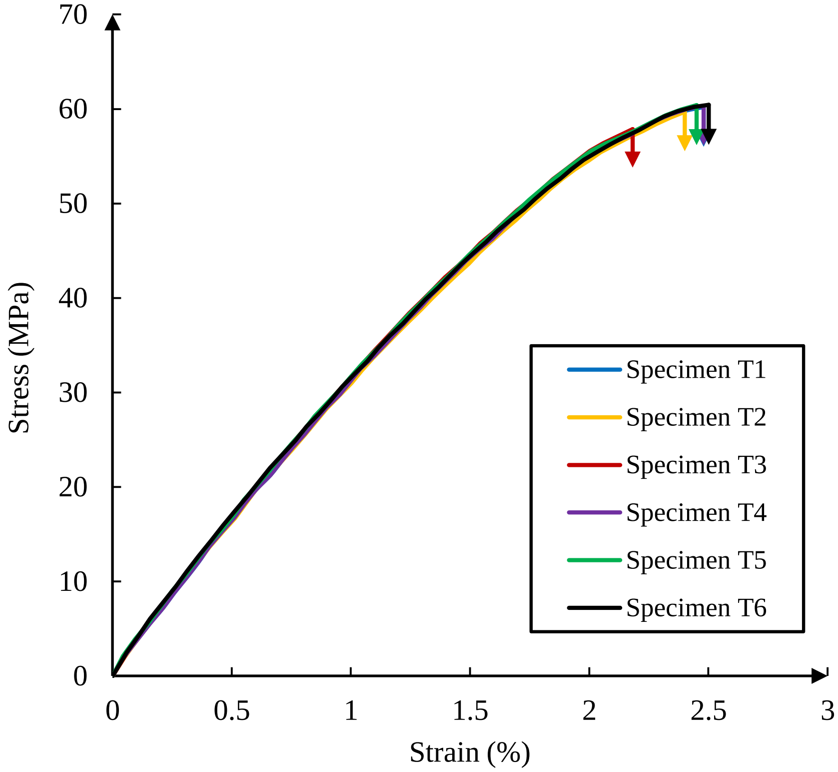

Figure 3.8 - Stress-strain curves for uniaxial load testing.

Slight variations in both stress and strain failure limits were observed. Table 3.2 documents the failure limits of each specimen and the fracture energy from testing results. The mean values of elastic constants, namely modulus of elasticity and Poisson's ratio were 3.328 GPa and 0.361, respectively.

Table 3.2. Failure limits from uniaxial tension testing.

specimen number	failure stress (MPa)	failure strain (%)	fracture energy (N/m)
T1	53.82	2.187	1.885
T2	59.70	2.401	2.039
T3	60.22	2.481	2.108
T4	60.35	2.482	2.018
T5	60.46	2.502	2.114
T6	60.42	2.452	2.101

The DIC local measurements of regarding load-displacement results are shown in Figure 3.9. Local measurements showed similar plateau to that of global ones. Specimen T5 showed the maximum local displacement and load at failure as 687μm and 4734N, respectively. The lowest values were recorded by specimen T1 as 551μm and 4546N.

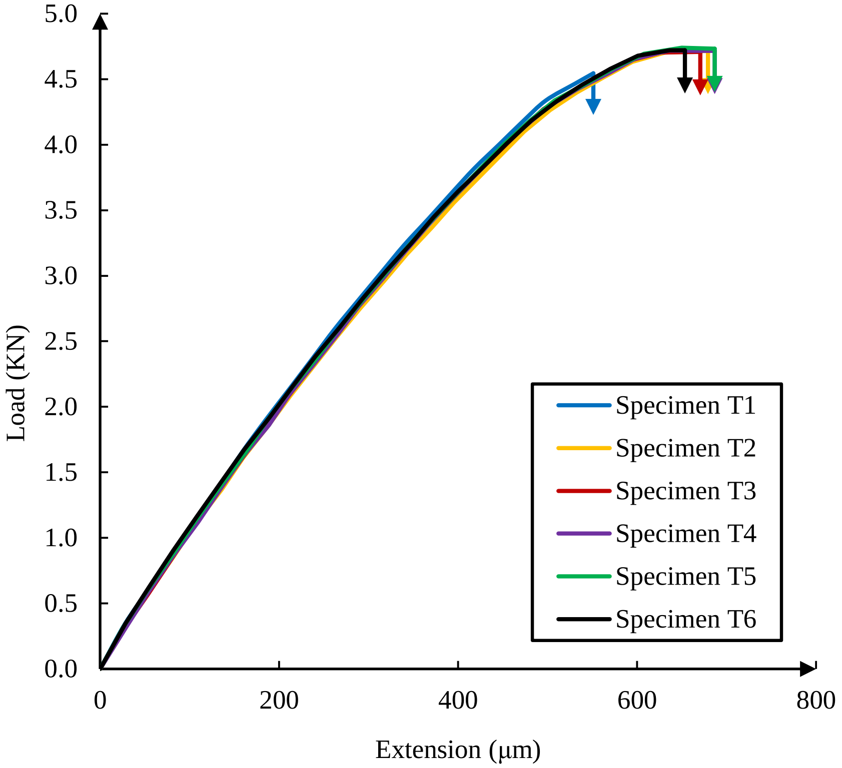

Figure 3.9 - Local axial load-displacement measurements from DIC.

Fractured specimens from uniaxial tension testing were scanned, and monochromic images are presented in Figure 3.10. All specimens showed a fractured surface normal to load application direction implying that brittle type of failure dominated the fracture mechanism. Even though plastic deformation was minimal, stress-whitening caused by plastic deformation can be observed in all specimens.

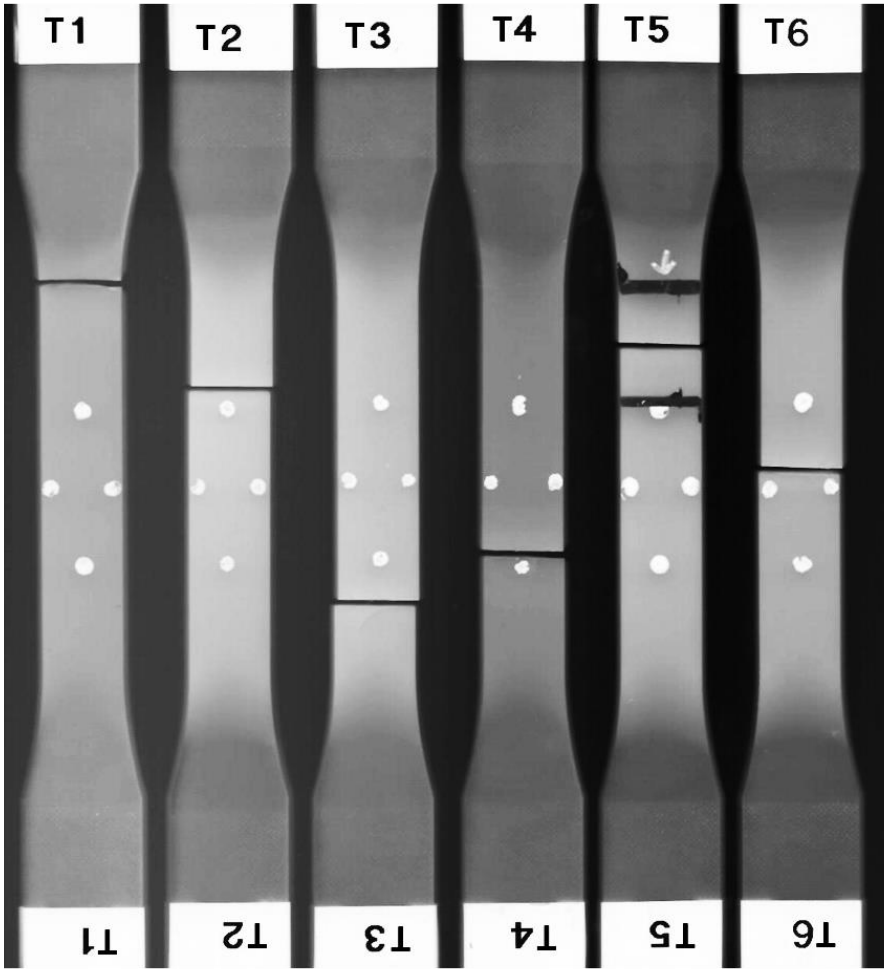

Figure 3.10 - Monochromic scan of dog-bone specimens after failure.

3.5 Simulation Results and Discussion

Table 3.3 – Simulation and experimental test results

Property	22%	52%	66%	76%	Experimental
Young's Modulus (GPa)	2.82	3.33	3.95	4.28	3.328
Standard Deviation (GPa)	0.50	0.61	0.82	0.60	
Poisson's Ratio	0.381	0.381	0.377	0.354	0.361
Standard Deviation	0.016	0.018	0.026	0.027	
Density (g/mL)	1.132	1.139	1.139	1.140	1.10
Standard Deviation (g/mL)	0.004	0.003	0.004	0.003	

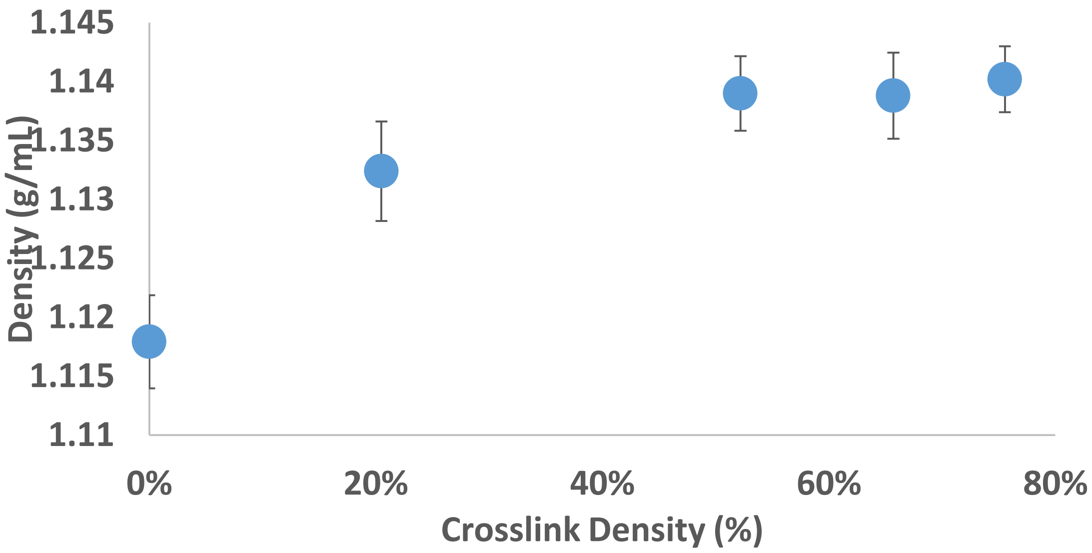

Figure 3.11 – Average density of samples as a function of crosslink density.

The density of the epoxy samples are shown as a function of degree of cure in Figure 3.11. The densities are sampled at a temperature of 300 K and a pressure of 1 atm. For each sample at all crosslink densities, the densities are noticeably higher than that of the equilibrated, unreacted mixes. As crosslinking density increases the trend shows density slightly increases. This is expected since as more bonds form, the monomers become held more tightly together, and thus density will increase. The density increases the most between 0 to 22% crosslink density, and changes very little after 50% reaction completion. The average measured density of the epoxy samples is 1.10 g/mL which is in good agreement with the simulation. Overall the MD simulations overestimate the density.

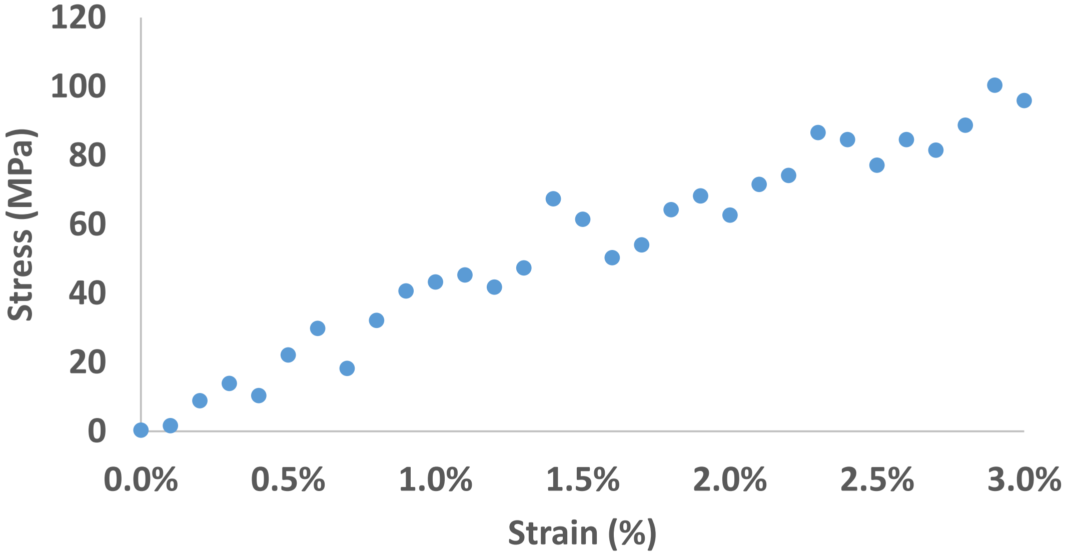

Figure 3.12 – Stress-strain curve obtained from simulation of a 22% crosslink density system

Figure 3.12 above is a typical stress-strain curve obtained through the MD simulations. Young's Modulus is estimated using the first 1.5 – 2.0% strain of the curve based on how linear the section is, as well as to reflect the elastic limit of the experimental results. The CVFF force field does not allow for bond breaking due to applied force, and thus is not a suitable potential for estimating yield strength and fracture strength, and the focus will be on the accuracy of Young's Modulus and Poisson's Ratio. The average predicted Young's Modulus for different crosslink densities is shown in Figure 3.13 along with the standard deviation of each degree of cure. Young's modulus was found to increase with an increasing degree of cure, which shows the model becomes stiffer as more bonds form. The MD simulations are in good agreement with the experimental modulus, with the value of 3.328 GPa falling within the range of crosslink density for 22-66%. Typical final degree of cures for similar epoxy systems tend to be in the range of 70-85% cured, which would imply these simulations are slightly overestimating the modulus [22]. This is a common trend in MD modelling of epoxies and can be attributed to the fact that these simulations have no defects present such as impurities and voids [23]. The average standard deviation for Young's Modulus is 0.63 GPa, which is in agreement with the variance found in other simulations with similar epoxies [18].

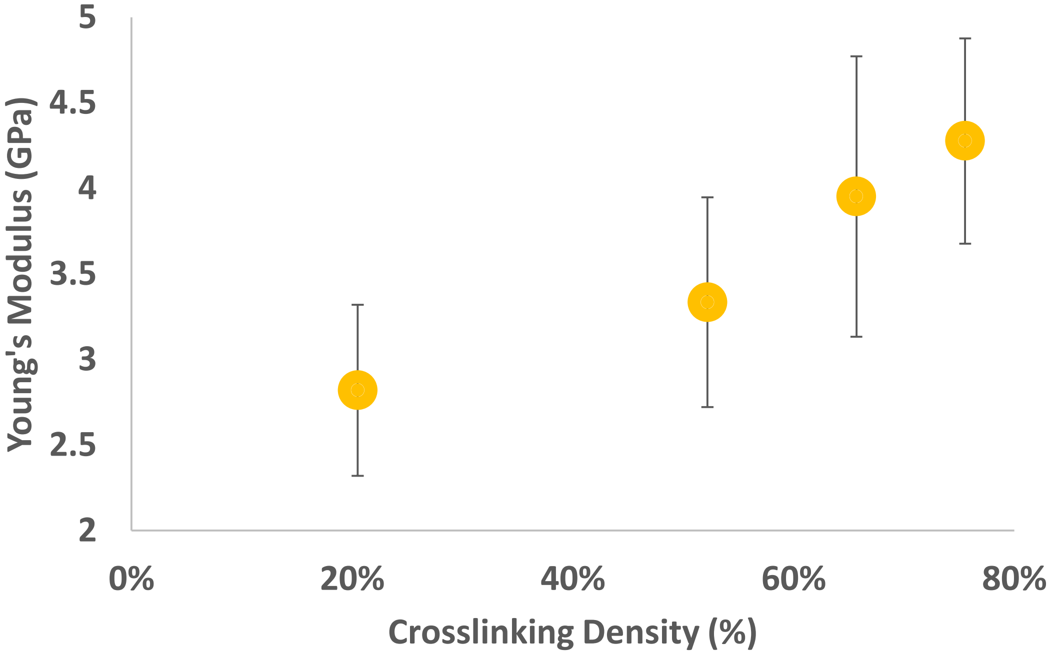

Figure 3.13 – Young's Modulus obtained from simulation at different crosslink densities.

Poisson's ratio is calculated by recording the two transverse strains during the tensile test procedures and comparing each to the axial strain. Poisson's ratio for each sample is taken as the average value extracted from the three tensile tests performed. The average value for each crosslink density along with its standard deviation is presented in Figure 3.14. The model shows that Poisson's ratio has little dependence on the crosslink density, and tends to slightly decrease as reaction completion increases.

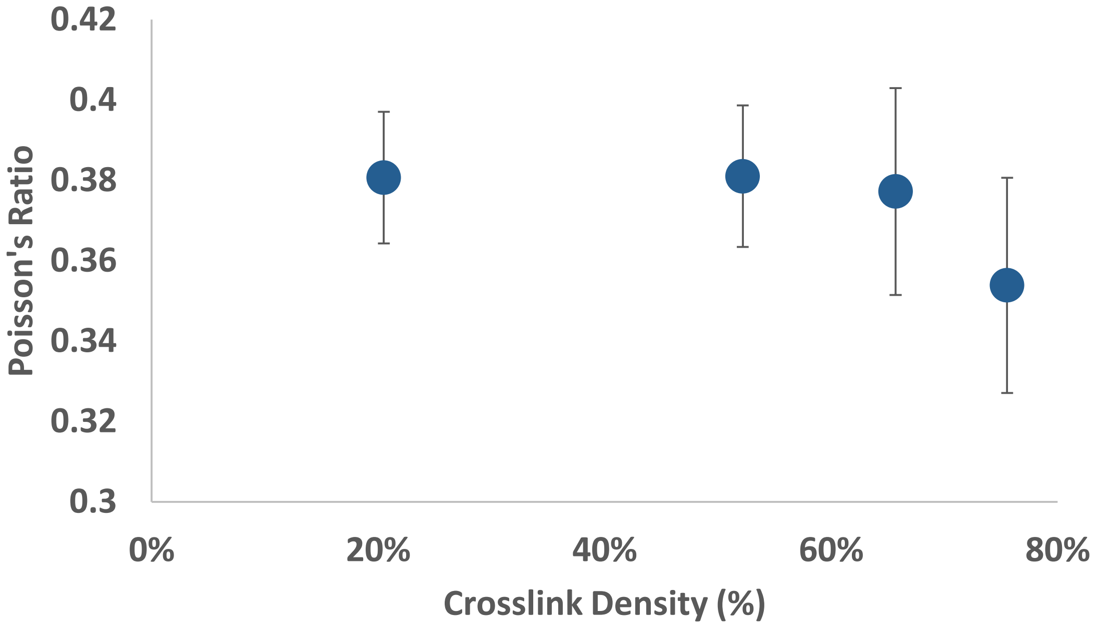

Figure 3.14 – Results for Poisson's Ratio obtained from simulation as a function of crosslink density.

3.6 Conclusions

This MD study examined the mechanical properties as a function of crosslinking for the DGEBA/DETDA polymer system. Different degrees of crosslinking ranging from 25% to a maximum value of 76% were observed. Young's Modulus was found to increase with increasing crosslink density. Density also increased with increasing reaction completion between 0 and 50% then saw little change with further crosslinking. Poisson's

Ratio was not significantly affected by increasing crosslink density, slightly decreasing as it approached the maximum degree of crosslinking. From these simulations the Young's Modulus, Poisson's ratio and density were estimated and compared to the experimental results. All three properties were found to be in good agreement with the polymer simulations. The good comparison with the experimental shows the crosslinking procedure proposed here is suitable for modelling epoxy polymers, providing a simpler method for modeling the curing process of DGEBA and DETDA.

References

[1] J. L. Massingill and R. S. Bauer, "Epoxy Resins," in Craver C.D.; Carraher Jr. C.E., Eds, Applied Polymer Science 21st Century, Elsevier, Amsterdam, pp. 393-424, 2000. . DOI: https://doi.org/10.1016/B978-008043417-9/50023-4.

[2] W. Brostow, S. H. Goodman and J. Wahrmund, "Epoxies," Handbook of Thermoset Plastics /, pp. 191-252, 2014. . DOI: 10.1016/B978-1-4557-3107-7.00008-7; info:doi/10.1016/B978-1-4557-3107-7.00008-7.

[3] J. A. Brydson, "Epoxide Resins," Plastics Materials, Seventh Edition, pp. 744-777, 1999. . DOI: 10.1016/B978-075064132-6/50067-X; info:doi/10.1016/B978-075064132-6/50067-X.

[4] S. H. Goodman and H. Dodiuk, Handbook of Thermoset Plastics, Third Edition. (3rd ed ed.) 2014. DOI: 10.1016/C2011-0-09694-1.

[5] F. Jeyranpour, G. Alahyarizadeh and B. Arab, "Comparative investigation of thermal and mechanical properties of cross-linked epoxy polymers with different curing agents by molecular dynamics simulation," J. Mol. Graph. Model., vol. 62, pp. 157-164, 2015.

[6] G. Levita et al, "Crosslink density and fracture toughness of epoxy resins," J. Mater. Sci., vol. 26, (9), pp. 2348-2352, 1991. . DOI: 10.1007/BF01130180.

[7] D. K. Chattopadhyay, S. S. Panda and K. V. S. N. Raju, "Thermal and mechanical properties of epoxy acrylate/methacrylates UV cured coatings," Progress in Organic Coatings, vol. 54, (1), pp. 10-19, 2005. . DOI: 10.1016/j.porgcoat.2004.12.007.

[8] I. Yarovsky and E. Evans, "Computer simulation of structure and properties of crosslinked polymers: application to epoxy resins," Polymer, vol. 43, (3), pp. 963-969, 2002.

[9] K. Fu et al, "Molecular Dynamics Simulation and Experimental Studies on the Thermomechanical Properties of Epoxy Resin with Different Anhydride Curing Agents," Polymers, vol. 11, pp. 975, 2019. . DOI: 10.3390/polym11060975.

[10] A. Bandyopadhyay et al, "Molecular modeling of crosslinked epoxy polymers: The effect of crosslink density on thermomechanical properties," Polymer, vol. 52, (11), pp. 2445-2452, 2011. . DOI: https://doi.org/10.1016/j.polymer.2011.03.052.

[11] M. S. Radue and G. M. Odegard, "Multiscale modeling of carbon fiber/carbon nanotube/epoxy hybrid composites: Comparison of epoxy matrices," Composites Sci. Technol., vol. 166, pp. 20-26, 2018. . DOI: 10.1016/j.compscitech.2018.03.006.

[12] C. Li and A. Strachan, "Molecular simulations of crosslinking process of thermosetting polymers," Polymer, vol. 51, (25), pp. 6058-6070, 2010.

[13] A. Gavrielides et al, "Model of the DGEBA-EDA Epoxy Polymer: Experiments and Simulation Using Classical Molecular Dynamics," International Journal of Polymer Science, vol. 2019, 2019.

[14] V. Varshney et al, "A molecular dynamics study of epoxy-based networks: cross-linking procedure and prediction of molecular and material properties," Macromolecules, vol. 41, (18), pp. 6837-6842, 2008.

[15] L. Tam and D. Lau, "A molecular dynamics investigation on the cross-linking and physical properties of epoxy-based materials," RSC Advances, vol. 4, (62), pp. 33074-33081, 2014.

[16] S. Plimpton, "Fast Parallel Algorithms for Short- Range Molecular Dynamics," Journal of Computational Physics, vol. 117, (1), pp. 1-19, 1995. . DOI: 10.1006/jcph.1995.1039.

[17] A. Stukowski, "Visualization and analysis of atomistic simulation data with OVITO–the Open Visualization Tool," Modell Simul Mater Sci Eng, vol. 18, (1), pp. 015012, 2009.

[18] M. S. Radue et al, "Comparing the mechanical response of di-, tri-, and tetra-functional resin epoxies with reactive molecular dynamics," Journal of Polymer Science Part B: Polymer Physics, vol. 56, (3), pp. 255-264, 2018.

[19] S. V. Kallivokas, A. P. Sgouros and D. N. Theodorou, "Molecular dynamics simulations of EPON-862/DETDA epoxy networks: structure, topology, elastic constants, and local dynamics," Soft Matter, vol. 15, (4), pp. 721-733, 2019.

[20] J. R. Gissinger, B. D. Jensen and K. E. Wise, "Modeling chemical reactions in classical molecular dynamics simulations," Polymer, vol. 128, pp. 211-217, 2017.

[21] A. Y. Elruby and S. Nakhla, "Strain energy density based damage initiation in heavily cross-linked epoxy using XFEM," Theor. Appl. Fract. Mech., vol. 103, pp. 102254, 2019.

[22] H. Dannenberg and W. Harp, "Determination of cure and analysis of cured epoxy resins," Anal. Chem., vol. 28, (1), pp. 86-90, 1956.

[23] N. B. Shenogina et al, Molecular Modeling of Thermosetting Polymers: Effects of Degree of Curing and Chain Length on Thermo-Mechanical Properties, 2012.

4. Chapter 4: Summary

The work performed in the previous chapters shows the capabilities of Molecular Dynamics as a method for predicting mechanical properties of structural materials. The use of simulations offers a cheaper and less resource-intensive method for material testing compared to the cost and time of instrumentation and performing experiments. Furthermore, MD simulations offer the insight to material phenomena on the micro- and nanoscale that can't be easily explained through experimental or spectroscopic techniques. The use of nanoindentation simulations can be used to model the atom movement and plastic deformation pathways that can't be observed through actual testing. As for polymers, atomistic simulations can show how the crosslink reaction during curing directly correlates to desired mechanical properties, as well as offer a simple method to compare the performance of different resin and hardener monomers. As discussed, actual testing and development of new resins is a time consuming and costly process. The MD simulation approach has been shown to accurately predict properties of known epoxies and could be applied to the research and development of new polymers.

In Chapter 2, the author of this thesis has tested the applicability of available force fields to the use of nanoindentation. The author found that not all force fields tuned for elastic properties were appropriate for predicting elastic modulus through this technique. The best force fields using the Oliver & Pharr method could predict the modulus aluminum within 13% error. The simulation results were compared to the literature for single crystal aluminum.

For Chapter 3, the author has detailed a procedure for building large atom epoxy models for the DGEBA/DETDA system that could be extended to any organic polymer. The results of the virtual tensile test were in good agreement with the experimental results performed. The model showed the polymer’s elastic modulus and density were significantly influenced by the degree of cure.